



## Agent-based system identification for control-oriented building models

Jaewan Joe & Panagiota Karava

To cite this article: Jaewan Joe & Panagiota Karava (2017) Agent-based system identification for control-oriented building models, *Journal of Building Performance Simulation*, 10:2, 183-204, DOI: [10.1080/19401493.2016.1212272](https://doi.org/10.1080/19401493.2016.1212272)

To link to this article: <https://doi.org/10.1080/19401493.2016.1212272>



Published online: 18 Aug 2016.



Submit your article to this journal



Article views: 491



View related articles



View Crossmark data



Citing articles: 6 View citing articles

## Agent-based system identification for control-oriented building models

Jaewan Joe<sup>a,b</sup> and Panagiota Karava<sup>a,b\*</sup>

<sup>a</sup>Lyles School of Civil Engineering, Purdue University, 550 Stadium Mall Dr., West Lafayette, IN 47907, USA; <sup>b</sup>Center for High Performance Buildings, Ray W. Herrick Laboratories, 140 S. Martin Jischke Dr., West Lafayette, IN 47907, USA

(Received 25 March 2016; accepted 9 July 2016)

The paper presents a general agent-based system identification framework as potential solution for data-driven models of building systems that can be developed and integrated with improved efficiency, flexibility and scalability, compared to centralized approaches. The proposed method introduces building sub-system agents, which are optimized independently, by solving locally a maximum likelihood estimation problem. Several models are considered for the sub-system agents and a systematic selection approach is established considering the root mean square error, the parameter sensitivity to output trajectory and the parameter correlation. The final model is integrated from selected models for each agent. Two different approaches are developed for the integration; the negotiated-shared parameter model, which is a distributed method, and the free-shared parameter model based on a decentralized method. The results from a case-study for a high performance building indicate that the model prediction accuracy of the new approach is fairly good for implementation in predictive control.

**Keywords:** system identification; agent-based estimation; distributed and decentralized methods; grey-box models; plug-and-play

### 1. Introduction

Advanced supervisory control strategies, such as model predictive control (MPC), have the potential to address the growing complexity of control requirements of modern buildings, considering their specific energy and comfort delivery features and the local climate, while facilitating the deployment of transaction-based interactions with the energy grid. To date, research on MPC of buildings has been mainly carried out in simulation environments (Braun, Montgomery, and Chaturvedi 2001; Cigler et al. 2012; Corbin, Henze, and May-Ostendorp 2012; Feng et al. 2015; Hu and Karava 2014; Lehmann et al. 2013; Li et al. 2015; Oldewurtel et al. 2012; Sourbron, Verhelst, and Helsen 2013; Sun et al. 2010). Experimental and field studies, despite being the exception rather than the rule, show promising results (Bengea et al. 2014; De Coninck and Helsen 2016; Ma, Borrelli, and Hencey 2012; Ma et al. 2012; Ma, Matuško, and Borrelli 2014; Široký et al. 2011; West, Ward, and Wall 2014). In previous studies has been concluded that the pathway of obtaining a suitable model that can be implemented in a predictive controller is time-consuming, corresponding to around 70% of the project engineering cost (Henze 2013), and not easily repeatable. Developing control-oriented models through a system identification approach, based on actual experiments, can be a long process particularly

for high performance buildings due to the large number of sub-systems for energy and comfort delivery and the increased complexity of the integrated building system and its dynamic behaviour. In such cases, the model structure typically includes a large number of estimate parameters, increasing the computational time and impeding finding a global minimum. Also, various sub-systems form a multiple input and multiple output (MIMO) system entailing different characteristics of dynamics in each sub-system; thereby, a centralized parameter estimation approach is hardly feasible for this case. For buildings with complex systems for better performance, it is possible to utilize their modularity to deploy plug-and-play approaches that improve efficiency, flexibility and scalability. Plug-and-play concepts can be realized with agent-based methods, that is, a special class of distributed approaches that enables parallel estimation of each sub-system and control of coupled but separable (due to sparsity) sub-systems that are jointly optimized. Decomposition methods are used to solve a large-scale optimization problem by breaking it up into smaller sub-problems with lower dimension of variables, and solving the sub-problems independently. In order to coordinate the solution of the sub-problems, a network of intelligent agents is formed, in which, the sub-system solvers are equipped with the capability of collaborating with other sub-system solvers, for

\*Corresponding author. Email: [pkarava@purdue.edu](mailto:pkarava@purdue.edu)

example, exchanging parameters, sharing data, negotiating strategies, etc. (Jennings and Bussmann 2003; Necoara, Nedelcu, and Dumitache 2011; Negenborn and Maestre 2014; Samar, Boyd, and Gorinevsky 2007).

Agent-based methods have been applied to building control problems. Several studies are concept-based, focused on defining the agents and their functions (Davidson and Boman 2005; Duan and Fan Lin 2008; Kelly and Bushby 2012; Mo 2003; Sharples, Callaghan, and Clarke 1999; Simoes and Bhattacharai 2011; Treado 2010; Treado and Delgoshaei 2010; Zhao, Suryanarayanan, and Simões 2013). Other studies considered actual buildings to demonstrate the application of decomposition methods (Cai et al. 2015; Ma, Anderson, and Borrelli 2011; Moroşan et al. 2010b), manage the needs and resources (Lacroix, Ines, and Mercier 2012; Mokhtar et al. 2013; Yang and Wang 2013), and exchange information of room air temperature trajectory between adjacent zones (Moroşan et al. 2010a; Putta et al. 2014). Our literature review shows that very few studies have developed estimation frameworks in sensor networks of complex systems, based on distributed optimization (Necoara, Nedelcu, and Dumitache 2011; Samar, Boyd, and Gorinevsky 2007). Also, this approach has not been exploited previously as a potential solution for control-oriented models of building systems that can be easier to develop and integrate. This distributed formulation is distinct from the control application in the sense that it is a static problem in terms of the estimate parameters and could be easily generalized to other cases where the controller type is identical.

The objective of this study is to develop and demonstrate, for the first time, an agent-based framework for data-driven grey-box building models. This includes identifying agents, their function and network structure, and estimating model parameters for both individual agents in the system, using information locally known or observable by each agent, and their connections. In the proposed framework, each sub-system agent uses information from sensors to solve a smaller-scale estimation problem, with a lower number of parameters compared to centralized schemes. A classical decomposition approach, the dual decomposition, that takes advantage of the separable optimization problem with Lagrangian, is used to solve the maximum likelihood estimation problem in a distributed setting. Two methods are presented based on the distributed and decentralized estimation (Negenborn and Maestre 2014), resulting in a negotiated-shared parameter model and a free-shared parameter model respectively. The developed agent-based system identification framework is demonstrated using a case-study of an open-plan office space with multiple sub-systems (radiant floor, double façade, room) and uncontrolled occupant schedule.

The proposed framework utilizes the modularity of building sub-systems and has the following distinct advantages: (a) scalability: sub-system models can be developed and integrated in a plug-and-play manner, reducing the

building physics expertise and engineering cost that is required for control-oriented models of high performance buildings, such as those with complex energy and comfort delivery systems; (b) efficiency: each agent faces a smaller-scale problem compared to centralized identification schemes; (c) flexibility: agents form agent-networks that can be easily configured and dynamically re-configured in adaptation to system upgrades and retrofits.

In this paper, Section 2 presents background information on system identification and grey-box models along with important advances and limitations for building applications. The agent-based parameter estimation methodology is presented in Section 3 and results for its implementation for a case-study building in Section 4. Finally, conclusions and recommendations for future work are discussed in Section 5.

## 2. Background

Grey-box models are considered as robust controllers and have been adopted for many building applications (Bacher and Madsen 2011; Berthou et al. 2014; Braun and Chaturvedi 2002; Cai and Braun 2015; De Coninck and Helsen 2016; Hazyuk, Ghiaus, and Penhouet 2012; Jiménez, Madsen, and Andersen 2008; Kramer, van Schijndel, and Schellen 2013; Prívara et al. 2012, 2013; Reynders, Diriken, and Saelens 2014; Široký et al. 2011; Žáčeková, Váňa, and Cigler 2014). Their structure is fairly simple compared to white-box models implemented in building energy simulation tools, and thereby are suitable for implementation in MPC. Compared to black-box models, grey-box models require a shorter period of data for training (Braun and Chaturvedi 2002; Reynders, Diriken, and Saelens 2014) and preserve the physical meaning and insight of each parameter (Hazyuk, Ghiaus, and Penhouet 2012; Reynders, Diriken, and Saelens 2014). Also, grey-box models do not require training data for different control schemes unlike black-box models, whose prediction is hardly matched with the experimental data unless all control schemes and output ranges are reflected in the training period (Braun and Chaturvedi 2002; Hazyuk, Ghiaus, and Penhouet 2012). In some cases, a grey-box model has been utilized as an initial model and then transferred to a final autoregressive-moving-average model (ARMAX) (Jiménez, Madsen, and Andersen 2008), transfer function (Braun and Chaturvedi 2002; Hazyuk, Ghiaus, and Penhouet 2012) or Model Predictive Control Relevant Identification (MRI) model (Prívara et al. 2012, 2013; Žáčeková, Váňa, and Cigler 2014). Overall, complexities in the estimation problem are associated with the non-linearity between the estimate parameter and output trajectory, and non-convexity of the objective function. As a result, falling in many local minima is quite common and reaching a global minimum is a difficult and time-consuming task.

Several studies emphasize the advantages of grey-box models and show good agreement with results from building simulation programs such as EnergyPlus (Prívara et al. 2013) and TRNSYS (Berthou et al. 2014; Braun and Chaturvedi 2002; Li et al. 2015; Prívara et al. 2012; Sourbron, Verhelst, and Helsen 2013), Modelica (De Coninck et al. 2015; De Coninck and Helsen 2016; Reynaers, Diriken, and Saelens 2014) and white-box models developed in Matlab environment (Hazyuk, Ghiaus, and Penhouet 2012; Hu and Karava 2014). However, simulation studies have limitations with regards to their applicability to the actual building estimation problem. Features of building simulation that differentiate it from the actual building operation are: (a) Information of occupancy schedule and internal heat gain is available. (b) Sensing reflects the true value without consideration of sensor uncertainty and sensor error range. (c) All temperature points of the building envelope and equipment heat gain are available, which are unlikely to be measured in actual buildings. (d) Rich input excitation is feasible by triggering set-point variations to unrealistic bounds. (e) Heat transfer coefficients and material properties are perfectly known so initial estimate parameters are decided based on those. Other studies were based on experiments in test-cells with well-controlled environments that allow rich input excitation without occupant interruptions (Bacher and Madsen 2011). Also, good agreement with experimental data from an actual multi-zone building has been achieved allowing a rough approximation of the state by averaging the room air temperature from eight different zones (Braun and Chaturvedi 2002), and treating the internal heat gain as an additional estimate parameter (Braun and Chaturvedi 2002; Cai and Braun 2015).

Identifiability is an important consideration in data-driven modelling indicating if the identified set of estimated parameters represents unique values so it is considered as a true system (Ljung 1999). Local (or output) identifiability represents the sensitivity of the estimate parameter variation to the output trajectory for given training data, thus, it is dependent on the data and model structure simultaneously. It is quantitatively expressed by the information matrix and represents the degree of the parameter influence to the output trajectory:

$$\frac{\partial \hat{Y}(\theta)^T}{\partial \theta} \frac{\partial \hat{Y}(\theta)}{\partial \theta} \in \mathbb{R}^{m \times m}.$$

$\hat{Y}$ ,  $\theta$  and  $m$  represent the output trajectory, estimate parameter and number of estimate parameters. Local identifiability is guaranteed by the full rank of information matrix, which means all parameters affect the output trajectory. Structure identifiability is not related to the training data but the model structure. It represents the parameter variation to output trajectory given zero initial state and zero input except initial input of one; each element of output

trajectory is expressed with Markov parameter sequence:

$$\frac{\partial M(\theta)}{\partial \theta} \in \mathbb{R}^{n \times 1},$$

where:

$$M(\theta) = [C(\theta)B(\theta) \quad C(\theta)A(\theta)B(\theta) \\ \dots C(\theta)A(\theta)^{n-1}B(\theta)].$$

$M$  and  $n$  represent Markov parameter sequence and number of iteration.  $A$ ,  $B$  and  $C$  represent matrices of state-space formulation. A model is structural identifiable when the structure identifiability matrix is full rank. Local identifiability and structure identifiability have been studied theoretically (Doren et al. 2009) and a systematic experiment design for the building estimation problem has been proposed to increase the identifiability (Agbi, Song, and Krogh 2012). A recent study for a building estimation problem used the identifiability to reduce the number of estimate parameters by fixing less identifiable parameters with defined thresholds (Cai and Braun 2015).

Correlation is another important consideration in estimation problems, and it is defined differently according to the associated variables such as the estimate parameter, input signal and residual. Parameter correlation refers to the correlated effects from two different parameters to the output trajectory; in case that two parameters give similar effects, the variation of one parameter is dependent on that of the other during the optimization process. A potential solution is transforming the parameter set to a less correlated that is a linear combination of the initial set, through principal component analysis (PCA). A theoretical discussion of the PCA method was presented in Del Barrio and Guyon (2003), followed by a building application example in Del Barrio and Guyon (2004). Similar studies were carried out to decorrelate the parameters by transforming their coordinates (Jiménez, Madsen, and Andersen 2008) or fixing the most correlated parameters one at a time with defined thresholds (Cai and Braun 2015). An implementable solution is providing sufficient input excitation during the experiment. Pseudo random binary sequence (PRBS) is a typical method, which has been widely used for building applications. It has been applied for grey-box models by exciting the heat input directly (Bacher and Madsen 2011; Hazyuk, Ghiaus, and Penhouet 2012) and black-box models by manipulating the set-point temperature (Li and Wen 2014; Royer et al. 2014). Rich excitation is feasible in simulation (Hazyuk, Ghiaus, and Penhouet 2012; Li and Wen 2014; Royer et al. 2014) and experimental studies in test-cells without actual occupants (Bacher and Madsen 2011), but sometimes it reaches unrealistic bounds (Bacher and Madsen 2011; Hazyuk, Ghiaus, and Penhouet 2012; Li and Wen 2014). A recent case-study found an optimal experiment

design for the input signal, which is turned out to be a bang-bang type, and reduced the data set size for estimation (Cai et al. 2016). Regarding the correlation originated from the inputs, signals of exogenous inputs such as the outdoor air temperature and solar radiation can be easily correlated. Including several days in the training data set with different weather conditions such as cloudy and sunny days resolves this issue. Finally, correlation analysis of the residual typically entails the auto-correlation and the cross-correlation between the input signal and residual, referred as whiteness and independence test respectively (Kramer, van Schijndel, and Schellen 2013). The auto-correlation function of the residual in simulation studies reveals that the residual is a white noise type (Jiménez, Madsen, and Andersen 2008; Reynders, Diriken, and Saelens 2014), which means that there is no missing input and the model structure is not too simple (Kramer, van Schijndel, and Schellen 2013). Strong cross-correlation between the input and the residual represents an incorrect model structure (Kramer, van Schijndel, and Schellen 2013). Previous studies have shown less cross-correlation in a simulation study where the uncertainty is not significant (Jiménez, Madsen, and Andersen 2008) and an experimental study of an actual building with free floating conditions (Kramer, van Schijndel, and Schellen 2013).

Based on this background information, several days with different weather conditions were used for the experiments conducted in this study to collect training data, in order to decorrelate the exogenous input signal. Also, an air temperature set-point was randomly selected from the comfort bound and implemented for a given time interval, to provide sufficient input excitation and to decorrelate the estimate parameters and increase their identifiability. For the grey-box model estimation, an approach using a sensitivity-based parameter range selection and range shift was implemented to avoid falling into a local minimum in the resulting non-linear and non-convex optimization problem. The local identifiability of each estimate parameter was quantified with the significance index for a given training data set, and utilized for the sub-system model comparison along with the correlation index based on the correlation coefficient of each two pairs of estimate parameters. The auto-correlation and cross-correlation functions were used to test the final estimated models as a post process technique.

### 3. Methodology

This section starts with the definition of the agent structure and then presents the formulation of the grey-box building sub-system models along with the methodology developed to improve the optimization process, and to establish the criteria for model quality. Finally, the shared parameter negotiation and agent-based estimation framework are described.

#### 3.1. Agent definition

In the proposed framework, each agent represents a building sub-system type: (a) terminal comfort delivery such as radiant heating/cooling system, chilled beam, under plenum air distribution; (b) building envelope (double façade, curtain wall, etc.); (c) zone, that is, space represented with a single zone or multiple sub-zones for local comfort delivery. Each agent in the multi-agent system can access only a portion of the sensors but has the ability to share data and communicate with its neighbouring agents. The integrated-system agent is assembled with information from sub-system agents. Also, there may be sensors deployed outside of the building for measuring and monitoring environment parameters (environment agent).

#### 3.2. Estimation of sub-system models

A grey-box model is formed from the heat balance equations on each node. An example for a temperature node is presented in Equation (1).  $X$ ,  $C_p$ ,  $R$  and  $Q$  represent the node temperature, the specific heat capacity, the resistance between two nodes and the heat flux input to the node, respectively.  $\alpha$  is the heat flux coefficient and represents the ratio of the thermal influence of each disturbance input to the state. The neighbouring temperature node is denoted as  $X_{adj}$ . Then the continuous time state-space equation is formulated with the state matrix  $A$ , input matrix  $B$ , state vector  $X$  and input vector  $u$  (Equation (2)). All environment data including outdoor air temperature and solar radiation as well as the controlled heating and cooling supply to the zone form the input vector  $u$ . Variables such as the capacity, resistance and heat flux coefficient  $\alpha$  form matrix  $A$  and  $B$ . The solution of this first-order ordinary differential equation is a discretized form of state-space equation assuming that the control inputs are constant for each time-step (Equation (3)). For this study, the time-step,  $k$ , is set to 5 min. The temperature of the next time-step is a linear function of the temperature and input at the current time-step and  $A_d$  and  $B_d$  matrix.

$$C_p \dot{X}_{node} = \sum \frac{X_{adj} - X_{node}}{R_{adj \sim node}} + \sum \alpha_{node} \dot{Q}_{node}, \quad (1)$$

$$\dot{X} = AX + Bu, \quad (2)$$

$$X_{k+1} = A_d X_k + B_d u_k. \quad (3)$$

In general, the grey-box estimation problem is not linear nor convex in terms of estimate parameter and output temperature trajectory. Statistically, the model structure is a maximum likelihood estimator (MLE) that requires prior information for each estimate parameter,  $\theta$ . A typical objective function is the summation of squared residual between the actual operation and the model prediction through all iterations,  $n$ . In this study, the square of the above function is used to expand the search space

(Equation (4)). The inverse of the capacity and resistance, and the heat flux coefficient, denoted with  $H$ ,  $U$  and  $\alpha$  (Equation (4)), are estimate parameters, so each element in  $A_d$  and  $B_d$  matrix of the discrete-time state-space equation is in the form of multiplication of variables.

$$\text{minimize} \left( \sum_{k=1}^n (\hat{y}[k] - y[k])^2 \right),$$

where:

$$\begin{aligned} X[k+1] &= A_d(\theta)X[k] + B_d(\theta)u[k], \\ \hat{y}[k] &= C_dX[k], \\ \theta &= [Cp_1^{-1}, \dots, Cp_{n_C}^{-1}, R_1^{-1}, \dots, R_{n_R}^{-1}, \alpha_1, \dots, \alpha_{n_\alpha}] \\ &= [H_1, \dots, H_{n_H}, U_1, \dots, U_{n_U}, \alpha_1, \dots, \alpha_{n_\alpha}]. \end{aligned} \quad (4)$$

The explicit matrix expression is shown in Equation (5). The estimation trajectory is a linear function of the initial state and input trajectory. The lower-triangle matrix with  $A_d$ ,  $B_d$  and  $C_d$  becomes larger as the estimation period is increased, and the estimation problem becomes more complex. Fmincon was used in Matlab environment among several optimization solvers for this constrained non-linear optimization problem. The active-set algorithm was selected (Mathworks 2015).

$$\text{minimize} ([\hat{Y}(\theta) - Y]^T [\hat{Y}(\theta) - Y])^2,$$

where:

$$\begin{aligned} \hat{Y}(\theta) &= \begin{bmatrix} \hat{y}[1] \\ \hat{y}[2] \\ \vdots \\ \hat{y}[n] \end{bmatrix} = \begin{bmatrix} C_d A_d(\theta) \\ C_d A_d(\theta)^2 \\ \vdots \\ C_d A_d(\theta)^n \end{bmatrix} x_0 \\ &+ \begin{bmatrix} (C_d B_d(\theta)) & 0 & \cdots & 0 \\ C_d A_d(\theta) B_d(\theta) & C_d B_d(\theta) & \cdots & 0 \\ \vdots & \vdots & \ddots & \vdots \\ C_d A_d(\theta)^{n-1} B_d(\theta) & C_d A_d(\theta)^{n-2} B_d(\theta) & \cdots & C_d B_d(\theta) \end{bmatrix} \\ &\times \begin{bmatrix} u[0] \\ u[1] \\ \vdots \\ u[n-1] \end{bmatrix}, \\ \theta &= [Cp_1^{-1}, \dots, Cp_{n_C}^{-1}, R_1^{-1}, \dots, R_{n_R}^{-1}, \alpha_1, \dots, \alpha_{n_\alpha}] \\ &= [H_1, \dots, H_{n_H}, U_1, \dots, U_{n_U}, \alpha_1, \dots, \alpha_{n_\alpha}]. \end{aligned} \quad (5)$$

This grey-box estimation has the following features: (a) large number of parameters including the resistance, capacitance and heat flux coefficient. (b) Large search region for each parameter; this large bound increases the chance to fall into a local minimum while there might be a global minimum. (c) Different sensitivity of each estimate parameter to the output trajectory so parameters require different

bounds, which requires trial and error based on intuition and engineering knowledge. Moreover, for the building estimation problem, typically a local minimum is found in the case of large air capacity that results in flat temperature when no or insufficient input excitation is given.

In this study, a sensitivity-based parameter range selection and range shift is implemented to update the parameter bound during the optimization process. In our approach, each parameter has a different search range that has the same sensitivity to the output so that optimal values are found based on impartial optimization for all parameters. Lower and upper bounds of each parameter are set with a bound range  $\gamma_p$  that gives the same perturbation to the output trajectory (Equation (6)). This is based on the standard deviation of the experimental output trajectory as follows:

$$[\theta_{p,LB}, \theta_{p,UB}] = [\theta_p^{\text{ini}} - \theta_p^{\text{ini}} \gamma_p, \theta_p^{\text{ini}} + \theta_p^{\text{ini}} \gamma_p],$$

where:

$$\begin{aligned} \gamma_p &= \arg \min_{\gamma \in [0, 0.99]} \\ &\times \left( Y_{\text{std}} - \sqrt{\frac{\hat{Y}(\theta_p^{\text{ini}} + \theta_p^{\text{ini}} \gamma)^T \hat{Y}(\theta_p^{\text{ini}} - \theta_p^{\text{ini}} \gamma)}{n}} \right)^2. \end{aligned} \quad (6)$$

Typically, the optimal parameter set is not inside the initial parameter range so a range shift method is introduced. The algorithm runs until all parameters are located inside the stop range  $\varepsilon$ , which is the ratio between the distance from the initial value and bound and the distance from the initial and optimal value in each iteration (Table 1). Figure 1 shows the parameter range shift algorithm for parameter  $\theta_p$ .  $k$  represents the time and the value of  $\varepsilon$  is 0.01 for this study. During the initial iterations, optimized values are close to the upper or lower bound while as the iterative process evolves parameter bounds are shifted with a different magnitude. In this way, the optimal value of each parameter is found based on different moving steps according to its significance. Finally, all parameters are inside the stop range and the iteration loop is terminated.

Table 1. Iteration loop for the parameter range shift.

---

while $ (\theta_p^{k+1} - \theta_p^k)/(\theta_{p,UB}^k - \theta_p^k)  < \varepsilon$ $\theta_p^{k+1} = \underset{\theta_p^k \in [\theta_{p,LB}^k, \theta_{p,UB}^k]}{\text{argmin}} ([\hat{Y}(\theta_p^k) - Y]^T [\hat{Y}(\theta_p^k) - Y])^2$ $[\theta_{p,LB}^{k+1}, \theta_{p,UB}^{k+1}] = [\theta_p^{k+1} - \theta_p^{k+1} \gamma_p, \theta_p^{k+1} + \theta_p^{k+1} \gamma_p]$ end
--

---

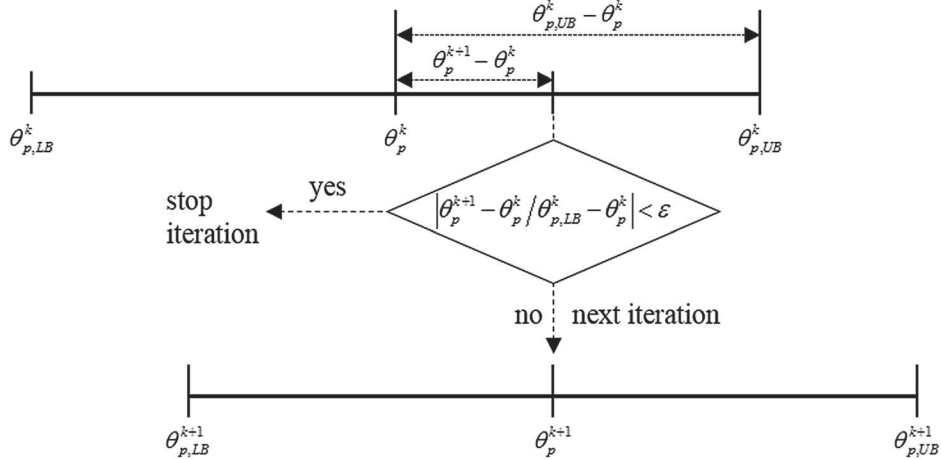


Figure 1. Graphical representation of the parameter range shift.

### 3.3. Criteria for model quality

The agent-based estimation approach developed in this study, is based on the optimization of sub-system models for which, each agent uses its own sensor and the experimental trajectory for the boundary temperature from its adjacent agent. The final model is assembled without further optimization. Therefore, accurate and robust models are required in the sub-system modelling step. In this regard, several criteria, including the prediction error, parameter significance and parameter correlation, are considered to select the best model among several candidates.

The root mean square error (RMSE) that shows the error intuitively while maintaining the actual unit of the output data was used for the comparison of each sub-system model.  $\hat{y}$ ,  $k$  and  $n$  in Equation (7) represent the model output, time and number of data.

$$\text{RMSE} = \sqrt{\frac{\sum_{k=1}^n (\hat{y}[k] - y[k])^2}{n}} = \sqrt{\frac{\hat{Y}Y}{n}}. \quad (7)$$

The models are also compared based on the significance index,  $SI_p$ . Sensitivity of the output trajectory from the model parameter variation is denoted as sensitivity matrix  $S$  based on the parameter perturbation method (Equation (8)) that enables the approximated calculation of sensitivity for the grey-box model where the output trajectory is not explicitly expressed with differentiable function according to each parameter (Del Barrio and Guyon 2003):

$$S_p = \frac{\partial \hat{Y}(\theta_p)}{\partial \theta_p} \approx \frac{\hat{Y}(\theta_p + \Delta\theta_p) - \hat{Y}(\theta_p)}{\Delta\theta_p}, \quad (8)$$

$$\tilde{S}_p = \theta_p S_p, \quad (9)$$

$$SI_p = \sqrt{\frac{\tilde{S}_p^T \tilde{S}_p}{n}}. \quad (10)$$

The variation of each parameter comes from the sensitivity-based parameter range  $\gamma_p$  discussed in Section

3.2. Herein  $\gamma_p$  is recalculated with the optimized value rather than the initial parameter. More specifically, 50% of the  $\gamma_p$  is multiplied with the parameter value ( $\Delta\theta_p = 0.5\gamma_p\theta_p$ ). For a fair comparison between parameters with different units, the reduced sensitivity matrix is used (Equation (9)) (Del Barrio and Guyon 2003). The significance index of parameter  $p$ ,  $SI_p$  is induced from the reduced sensitivity matrix, whose unit is  $^{\circ}\text{C}$  (Equation (10)).

Finally, the correlation index,  $CI_p$  (Equation (11)) is also introduced for the sub-system model comparison. The correlation coefficient shows how much each two parameters are correlated, which is denoted as  $\rho_{pq}$ . In this study, the Pearson product-moment correlation coefficient is used.  $K_{pq}$  and  $\sigma_p$  represent the covariance between two reduced sensitivities from two parameters of  $\theta_p$  and  $\theta_q$ , and the standard deviation of the reduced sensitivity from the parameter  $\theta_p$ .  $\tilde{S}_p$  and  $\tilde{S}_q$  represent column vectors consisting of averaged values of the reduced sensitivity matrices  $\tilde{S}_p$  and  $\tilde{S}_q$ . The obtained correlation coefficients are averaged for each parameter except that with itself, which is 1. In Equation (11)  $m$  represents the number of estimate parameters, and  $p$  and  $q$  represent the two pairs of estimate parameters. A model with parameters that have lower correlation index is considered to be superior.

$$CI_p = \frac{1}{m-1} \left( \sum_{q=1}^m \rho_{pq} - 1 \right),$$

where:

$$\begin{aligned} \rho_{pq} &= \frac{K_{pq}}{\sigma_p \sigma_q} \\ &= \frac{(\tilde{S}_p - \bar{S}_p)^T (\tilde{S}_q - \bar{S}_q)}{\sqrt{(\tilde{S}_p - \bar{S}_p)^T (\tilde{S}_p - \bar{S}_p)} \sqrt{(\tilde{S}_q - \bar{S}_q)^T (\tilde{S}_q - \bar{S}_q)}}. \end{aligned} \quad (11)$$

### 3.4. Shared parameter negotiation

In the agent-based estimation framework of this study, each agent has at least one sensor and boundary temperatures from neighbouring agents or environment data such as the outdoor air temperature. Figure 2 presents an example of an integration of two sub-system agents. Each sub-system agent has a parameter of resistance for a given physical location, named as shared parameter in this study (shared resistances are denoted with dotted lines in Figure 2). All sub-system agents are estimated independently, yielding different values of the shared parameter which are denoted as  $R_{23(i)}$  and  $R_{23(j)}$ . Since the final integrated-system agent requires one value ( $R_{23(int)}$ ) where a shared parameter exists, a parameter negotiation based on the dual decomposition is used to converge the different values from the sub-system model estimation to an identical value.

This type of distributed optimization problem is classified as Decoupled Cost but Coupled Constraints (DCCC) (Necoara, Nedelcu, and Dumitache 2011). Decoupled cost is formed when the sensors are installed for all sub-agents and coupled constraints are shared parameters between each neighbouring agent. In the dual decomposition method, the centralized optimization problem is transformed to Lagrangian dual function. The objective function of Lagrangian dual function consists of sub-problem's objective functions and consensus constraints of shared estimate parameters multiplied by the dual variable (Lagrangian multiplier). In this way, the problem is split into separate Lagrangian dual functions solved in parallel by updating the dual variables so the complicating (shared) variables are converged to the identical value (Nedíc and Ozdaglar 2009).

The typical dual decomposition without bounds for all iterations was not successful in our preliminary study because of the non-convex nature of the objective function. Therefore, lower and upper bounds for the shared parameters are set based on the assumption that the optimal value is located between two bounds which are the optimized

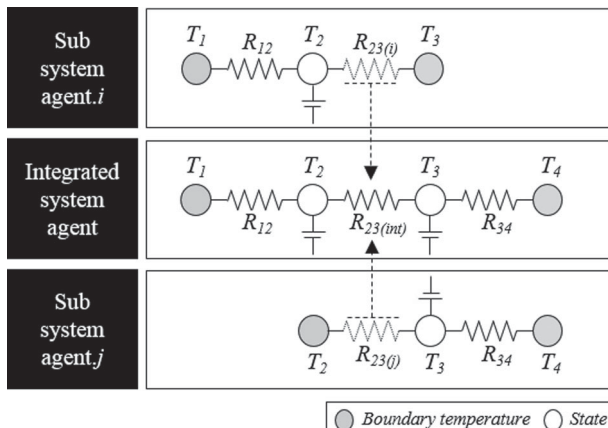


Figure 2. Example of sub-system and integrated-system agents.

Table 2. Dual decomposition algorithm for the negotiation between agent  $i$  and  $j$ .

---

```

while  $\theta_{ij(i)}^{k+1} = \theta_{ij(j)}^{k+1}$ 
 $\theta_i^{k+1} = \operatorname{argmin}_{\theta_i^k} (g_i(\theta_i^k) + \lambda_{ij}^k \theta_{ij(i)}^k)$ 
 $\theta_j^{k+1} = \operatorname{argmin}_{\theta_j^k} (g_j(\theta_j^k) - \lambda_{ij}^k \theta_{ij(j)}^k)$ 
 $\lambda_{ij}^{k+1} = \lambda_{ij}^k + \mu_{ij} (\theta_{ij(i)}^{k+1} - \theta_{ij(j)}^{k+1})$ 
end

```

---

values from the previous iteration. The dual decomposition algorithm for the negotiation between two sub-system agents  $i$  and  $j$  is shown in Table 2.  $\theta_{ij(i)}$  and  $\theta_{ij(j)}$  represent shared parameters that belong to agent  $i$  and  $j$ , respectively. A normalized form of the objective function  $g(\theta)$ , with a percentage of the relative difference between the optimal value from the sub-system agent  $f(\theta^*)$  and the current optimal value  $f(\theta)$ , was introduced for a fair optimization of each agent:

$$g(\theta^k) = 100 \left( \frac{f(\theta^k) - f(\theta^*)}{f(\theta^*)} \right). \quad (12)$$

The dual variable  $\lambda$  is linearly updated with the time-step  $\mu$  and the distance between the shared parameters  $\theta_{ij(i)}$  and  $\theta_{ij(j)}$ . The initial  $\lambda$  and the time-step  $\mu$  are set to 0 and 0.01, for this study.

### 3.5. Residual analysis

As discussed in Section 2 (Background), it may not be realistic to expect that the auto-correlation of the residual and cross-correlation between the input signal and residual based on experiments with the building in its actual operation mode (i.e. with uncertainty due to occupancy schedule, etc.) is inside the high confidence range. Therefore, in this study residual analysis does not represent an absolute criterion but provides some useful information as a post processing technique. The equations of auto-correlation (Equation (13)) and cross-correlation (Equation (14)) functions are shown below:

$$\hat{\rho}_{rr}(h) = \frac{\sum_{k=1}^{n-|h|} (r^{k+h} - \bar{r})(r^k - \bar{r})}{\sum_{k=1}^n (r^k - \bar{r})(r^k - \bar{r})}, \quad (13)$$

$$\hat{\rho}_{ru}(h) = \frac{\sum_{k=1}^{n-|h|} (r^{k+h} - \bar{r})(u^k - \bar{u}_i)}{\sum_{k=1}^n (r^k - \bar{r})(u^k - \bar{u})}. \quad (14)$$

$r$ ,  $u$  and  $h$  represent the residual between the experiment and prediction, input such as boundary temperature or heat flux, and the lag. Seventy-five per cent of the total estimation data length was set for the number of lags ( $h$ ) since

we use experimental datasets, although previous studies based on simulation used a significantly lower number (Bacher and Madsen 2011; Jiménez, Madsen, and Andersen 2008; Kramer, van Schijndel, and Schellen 2013). The confidence range was set based on 95% confidence band:  $\pm 1.96/\sqrt{n}$ .

### 3.6. Agent-based estimation

The agent-based estimation framework consists of two different methods; the negotiated-shared parameter and the free-shared parameter model, representing the distributed and decentralized approach respectively. Both start from sub-system model estimations. The outcome of the

distributed method is a typical grey-box model where physical interpretation of the shared parameters is incorporated; different shared parameters from sub-system model estimations are negotiated to be identical. In the decentralized approach, the outcome is a ‘pseudo grey-box’ model without physical interpretation, as two different shared parameters from the sub-system model estimations are maintained.

#### 3.6.1. Distributed method: negotiated-shared parameter model

Figure 3 presents the agent-based estimation framework of the distributed method. Sensor information and parameter

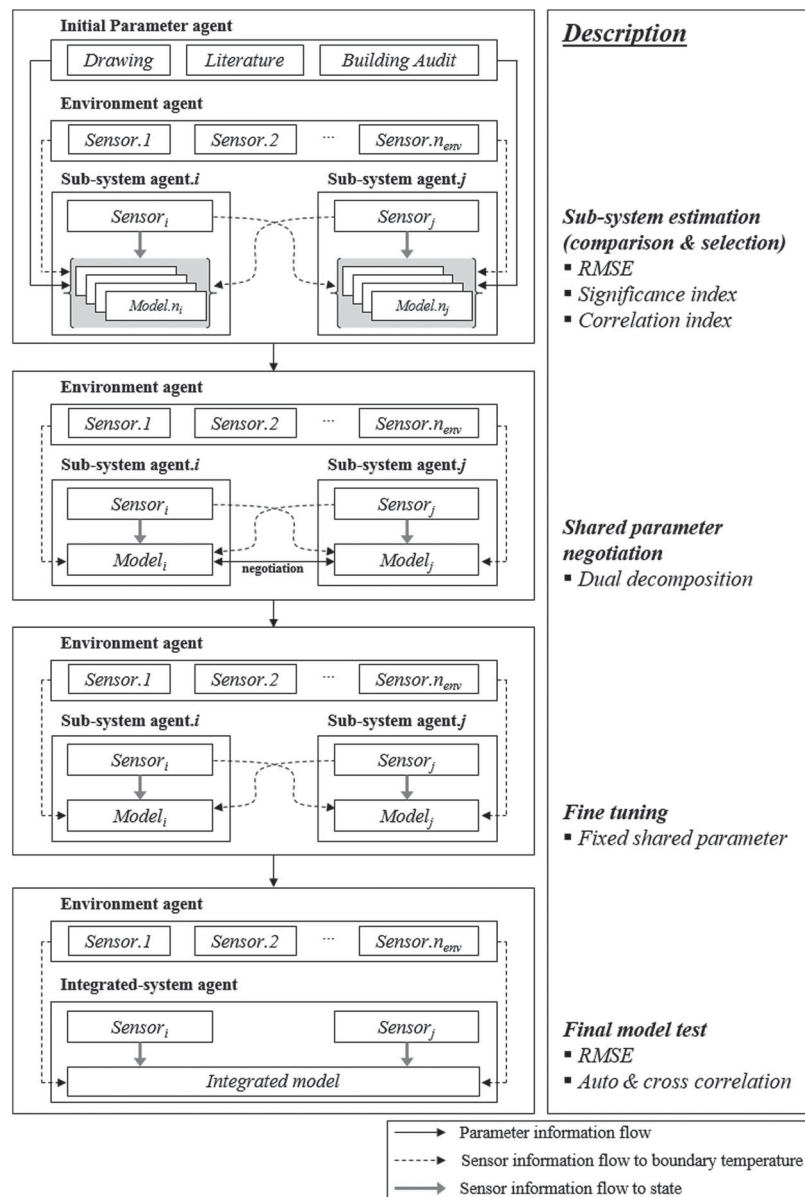


Figure 3. Agent-based estimation framework (distributed method).

information are delivered as shown by the dotted and solid arrow respectively. The initial estimate parameter  $\theta^0$  comes from the initial parameter agent, and may include information from the building drawings, literature, or a building audit. With this initial parameter, all sub-system models are estimated as discussed in Section 3.2. All models for each sub-system agent are compared to each other with three criteria including the RMSE, significance index  $SI$  and correlation index  $CI$ , and the best models are selected (Section 3.3). As each sub-system agent is optimized, the shared parameters for the selected best models are negotiated to be identical based on the dual decomposition method. In this step, the sensitivity-based parameter range is fixed at the final (optimized) value from the sub-system agent. Then, sub-system agent optimizations are carried out independently for fine tuning, by fixing the shared parameters to estimate the rest of the parameters, to improve the accuracy of sub-system models. Finally, the integrated model is assembled and tested with RMSE and residual analysis of auto-correlation and cross-correlation.

### 3.6.2. Decentralized method: free-shared parameter model

Figure 4 shows the information flow of the decentralized estimation. The initial steps are the same with the distributed estimation but the shared parameters are not negotiated. Therefore, coupled elements in off-diagonal parts of a state matrix have different value ( $R_{23(i)}$  and  $R_{23(j)}$ ) originate from each sub-system agent. A generic example, for the integrated-system agent in Figure 2, is shown in

Equation (15).

$$A = \begin{bmatrix} -\frac{1}{Cp_2} \left( \frac{1}{R_{12}} + \frac{1}{R_{23(i)}} \right) & \frac{1}{Cp_2} \left( \frac{1}{R_{23(i)}} \right) \\ \frac{1}{Cp_3} \left( \frac{1}{R_{23(j)}} \right) & -\frac{1}{Cp_3} \left( \frac{1}{R_{23(j)}} + \frac{1}{R_{34}} \right) \end{bmatrix}. \quad (15)$$

All sub-system agents are estimated independently using boundary temperatures for the adjacent agent from the experimental data. Thus, the integrated model yields good results once each sub-model shows good agreement with the experiment data. In other words, well-estimated sub-system models guarantee the prediction accuracy of the integrated model regardless of the agreement of shared parameters. However, the physical meaning of shared parameters is compromised.

## 4. Case-study

This section presents a case-study for the implementation of the agent-based system identification framework. It starts with a description of the test-bed and the data collection process and then presents the model estimation and selection for each sub-system and the integrated system.

### 4.1. Experiment

An open-plan office space (9.9 m by 10.5 m) that can host up to 20 occupants is a Living Laboratory and was considered as test-bed for this study (Figure 5). Its main features are a radiant floor slab and a south facing double façade

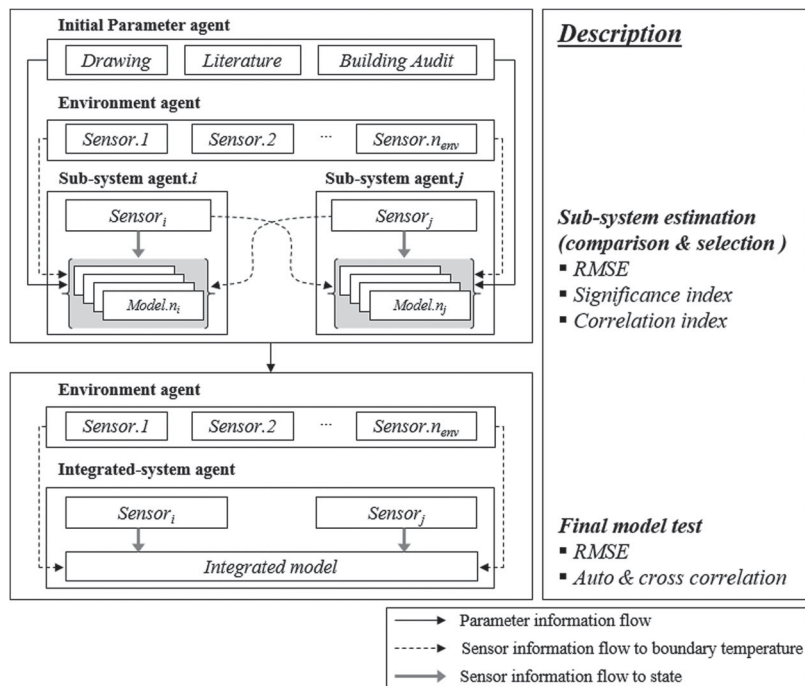


Figure 4. Agent-based estimation framework (decentralized method).



Figure 5. Exterior view of the building and test-bed (Living Lab 1).

system with 1.52 m cavity. A building management system (BMS) is available through the installed Tridium JACE controllers and Niagara/AX software framework (Tridium Inc), which in addition to a variety of internet-enabled features gives the ability to monitor, control and automate all the building systems regardless of manufacturer or communication protocols.

All sensor locations are illustrated in Figure 6 which presents a section view of the office. Details of the hydronic circuit for the radiant floor system are shown in Figure 7. Thermistors were used to measure the outdoor air temperature on the roof (BAPI, BA/10K-3,  $\pm 0.2\%$  @ 0–70°C), the cavity air temperature in the double façade (BAPI, BA/10K-3,  $\pm 0.2\%$  @ 0–70°C) and the room air temperature (BAPI, BA/BS2-WTH-SO,  $\pm 0.3^\circ\text{C}$  @ 25°C). The solar radiation was measured with two LI-COR 200-SL pyranometers (resolution of 0.1 W/m<sup>2</sup> and accuracy of 3%) mounted on the exterior glass surface (vertical) and the roof of the double façade (horizontal). Resistance temperature detectors (RTDs) were used for measuring the air temperature of the duct (ACI, A/TT1K-6,  $\pm 0.5\%$  @ 40–85°C), pipe water temperature of the radiant floor (ACI, A/TT1K-5,  $\pm 0.5\%$ ) and slab temperature inside the concrete (ACI, A/TT1K-LTS,  $\pm 0.3^\circ\text{C}$  @ 0°C). The slab is

divided into 10 sections. An RTD sensor with copper shielding is embedded at the centre of each section, around 1.9 cm from the top surface. The average reading of 10 RTD sensors was used for the estimation. The radiant floor in this office space has been constructed to provide local control and sensing capabilities, since this is a research Living Laboratory. In this study, although the average value of 10 RTD sensors was used, their difference was less than 1°C. Therefore, one or two sensors would be sufficient for this experiment and hence, the methodology can be generalized to typical buildings. The pipe circuit after the pump consists of 10 parallel loops in the concrete slab, which are merged prior to the heat exchanger (Figure 7). The supply and return water temperature was measured at the inlet and outlet side of the heat exchanger. The water flow rate was measured with a turbine flow meter (ONI-COM, F-1110,  $\pm 1$  @ 3–30 ft/s) installed before the heat exchanger.

Occupants (graduate students) have different schedules which was not monitored and no information was stored for the internal heat gains including the equipment and people except the power consumption of the electric lighting, which was measured in the BMS system. A roller shade installed on the inside surface of the window was fixed at a low position to decrease the uncertainty due to the solar

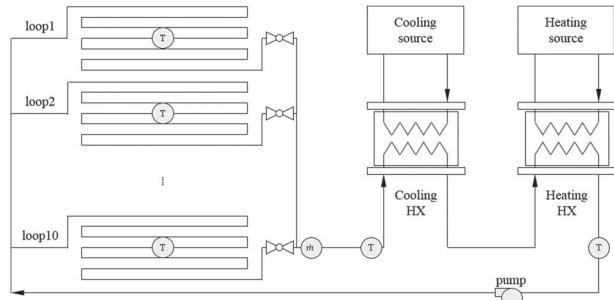


Figure 7. Hydronic circuit of the radiant floor system (notation: T and  $m$  represent the sensors for temperature and flow rate).

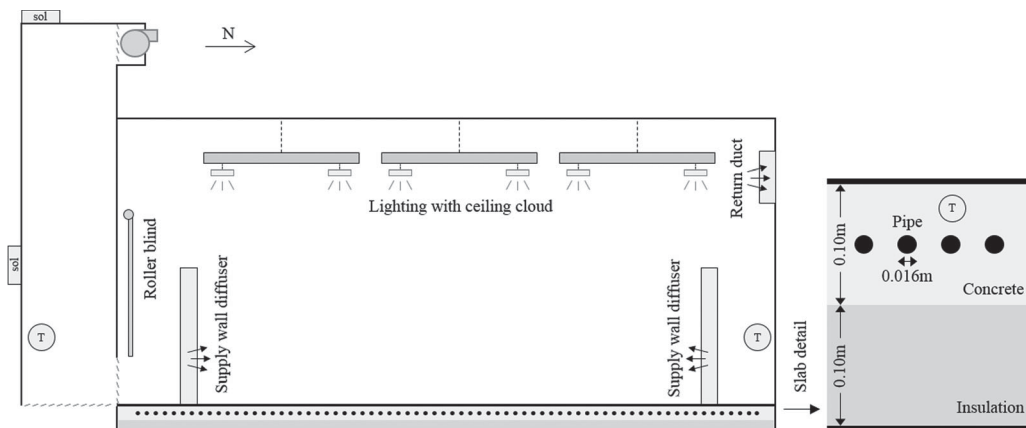


Figure 6. Section view of the open-plan office space with details of the floor slab (notation: T and sol represent the sensors for temperature and solar radiation).

gains and to eliminate the need to account for the time varying resistance between the cavity and room that was used in previous studies (Gwerder and Gyalistras 2013; Sun et al. 2010). The double façade has two vents on the lower section; one is between the cavity and outside and the other is between the cavity and the room. An exhaust fan with vent is located on the upper section of the façade. All vents were closed during the experiment and the fan was switched off so natural and mechanical ventilation in the cavity were not considered in this study. The room was conditioned using the radiant floor system by setting the supply water temperature with proportional-integral-derivative (PID) control so the air temperature set-point was met, while the water flow rate was fixed at 0.046 cubic meter per minute (12 gallon per minute), which is the maximum flow rate for the given pressure set-point of 0.69 bar (10 pound per square inch) of the pipe. The air temperature set-point was modified every 2 h, based on a randomly selected value between 21°C and 24°C. This is not the PRBS method but it was found to provide sufficient excitation to the system. The air handling unit (AHU) provides ventilation to the room with supply air temperature equal to the set-point temperature through three cylinder wall diffusers located in the three corners of the room and one rectangle wall diffuser on northern wall. Room air temperature, controlled by the radiant floor system, was not regulated well with variant set-point temperature due to the large capacity of the floor so heating and cooling was provided from the AHU and acted as a disturbance. The system identification experiment was carried out between June 1 and 20. Data collected during the first 5 days from the start of the experiment was used for estimation and data from the following 15 days for validation. The estimation set is followed by the validation set not to repeat the calculation of initial states where there is no sensor installed. All data were averaged every 5 min.

#### 4.2. Sub-system model estimation and selection

With a centralized estimation approach, a large number of estimate parameters, roughly between 12 and 24 depending on the model structure, is unavoidable. Also, each sub-system has different dynamics, for example, the magnitude of fluctuation of double façade air temperature is much larger than that of room air and slab temperature so the centralized estimation provides good results only for the double façade. Thus, in the agent-based approach, the single-zone building model is represented by three different sub-system agents, namely, the double façade agent, radiant floor agent and room agent.

In the modelling framework developed in this study, sub-system models are simplified linear state-space models that approximate with adequate resolution, the full dynamics; their structures represent a compromise between simplicity and preservation of physical sense. All parameters are time-invariant, temperature-independent, and some

of them are lumped according to the model structure. Unknown initial values for states without sensor measurements are estimate variables as well. Radiative heat transfers between surfaces are not considered. Initial conduction resistances are originated from the drawing when available, and capacitances are based on the air volume. Initial values of the heat flux coefficient ( $\alpha$ ) are calculated between 0 and 1, based on standard building properties and prior experience. For the significance index comparison of each sub-system model, all values are summed according to the estimate parameter type, that is,  $U$ ,  $H$  and  $\alpha$ . For the correlation index comparison of each sub-system model, averaged values along with the minimum and maximum of all estimate parameters are shown.

##### 4.2.1. Double façade agent

Two sub-system model structures are considered for the double façade agent including first- and second-order models (Figure 8).  $T_{cav}$  and  $T_{ext.win}$  represent the cavity temperature where the installed sensor is located and the exterior window surface temperature for which no sensor information is available. A third-order model that might have another state on the interior window between the cavity and the room is not considered in this study because the dynamics between two neighbouring agents is assumed to be represented with a time-invariant resistance without any state for the shared parameter negotiation. Boundary temperatures from the outdoor environment ( $T_{out}$ ) and the adjacent room agent ( $T_{room}$ ), along with the solar radiation ( $Q_{sol.ver}$ ) are used as known inputs. The heat flux input on each state is multiplied by the corresponding coefficient ( $\alpha_{sol.ext.win}$  and  $\alpha_{sol.cav}$ ). An initial value for the convective heat transfer coefficient on the double façade side was adopted from the literature (Park et al. 2004) and for the room side from TRNSYS type 56 (TRNSYS 17 2010). Figure 9 shows the model comparison for the double façade agent; it consists of five figures and the  $x$ -axis represents the model number. The first figure shows the RMSE of the estimation (E) and validation set (V). The second, third and fourth figures show the significance index of each parameter type, and the fifth figure shows the correlation

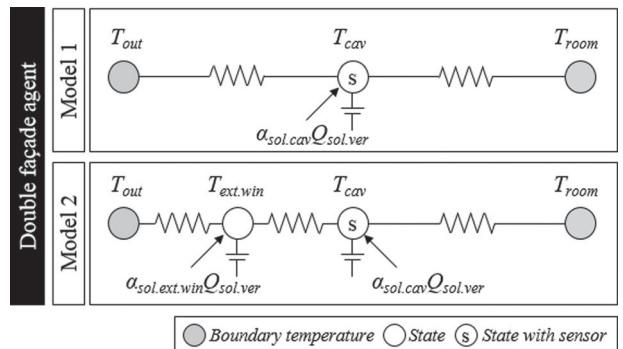


Figure 8. Structure of double façade agent models.

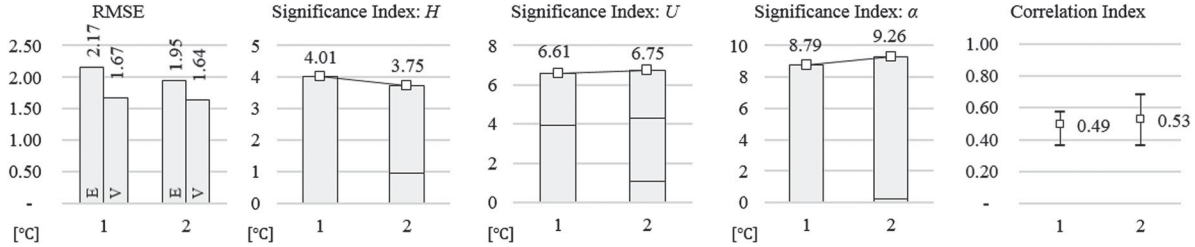


Figure 9. Model comparison of double façade agent (E and V represent estimation and validation).

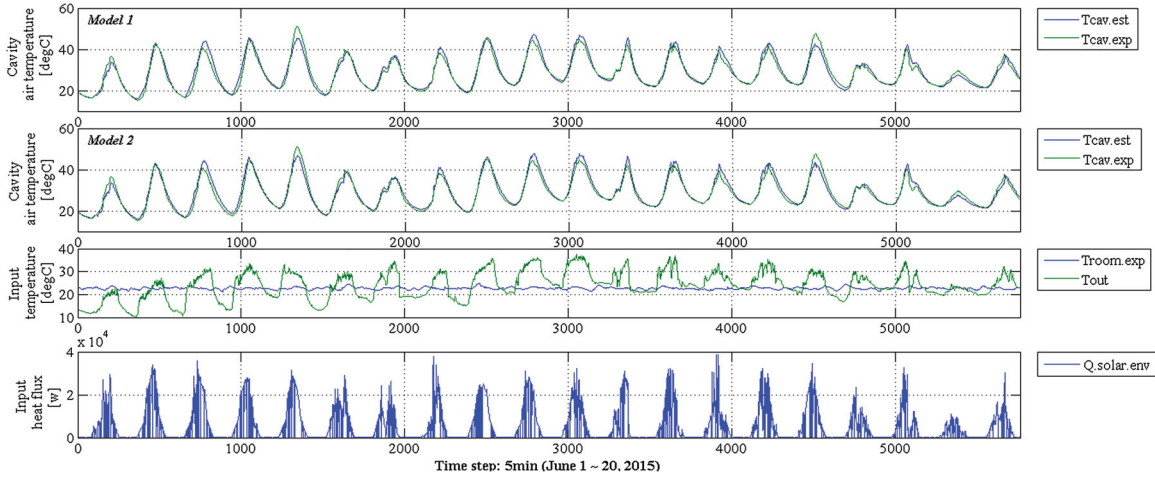


Figure 10. Estimation (1–1440) and validation (1441–5760) results for the double façade agent models.

index. Figure 10 shows the estimation (5 days, 1–1440) and validation (15 days, 1441–5760) results. Model 2 has lower error in the estimation period but the validation set shows almost the same accuracy for both models. The significance index does not provide a clear indication but parameters of model 1 are less correlated to each other. Model 1 with one state that does not require initial state information for unmeasurable points has been selected to be the best model.

#### 4.2.2. Radiant floor agent

Three sub-system model structures are considered for the radiant floor agent including two second-order models and a third-order model (Figure 11).  $T_{\text{slab}}$  represents the concrete temperature where the RTD sensors are located. In model 1 there is no additional parameter below  $T_{\text{source}}$  since there is insulation (10 cm) and air plenum (60 cm) below the slab so this boundary is assumed to be adiabatic. In model 2, constant temperature of 21°C for the adjacent zone in the floor below is considered ( $T_{\text{adj}}$ ) while model 3 has an additional state where the insulation and air plenum are located, denoted as  $T_{\text{sink}}$ . The air temperature from the room agent ( $T_{\text{room}}$ ) is the boundary input and the heat flux from the hot water to the concrete through the pipe ( $Q_{\text{rad}}$ ) is the controlled input. The disturbance inputs for the heat flux due to transmitted solar radiation and lighting ( $Q_{\text{sol.ver}}$  and  $Q_{\text{light}}$ ) are considered along with their

corresponding coefficients ( $\alpha_{\text{sol.slab}}$  and  $\alpha_{\text{light.slab}}$ ). Low-order models developed for radiant floor systems in the literature adopted a model structure with the hot water temperature as boundary input (Feng et al. 2015; Nghiêm et al. 2012; Nghiêm, Pappas, and Mangharam 2013; Široký et al. 2011; Sourbron, Verhelst, and Helsen 2013); some of them used the supply water temperature as a boundary temperature for control (Široký et al. 2011; Sourbron, Verhelst, and Helsen 2013) and others used the water flow rate with on/off control (Feng et al. 2015; Nghiêm et al. 2012; Nghiêm, Pappas, and Mangharam 2013). The model structure developed in this study has  $Q_{\text{rad}}$  as control input. In this way, both the supply water temperature and water flow rate could be controlled according to the sequence of  $Q_{\text{rad}}$ . All initial values including the conduction resistance and capacity are based on the design drawings. However, the exact material properties of concrete and insulation were not available, so assumptions were made, for example, the concrete and insulation types are typical, and the pipe is located in the middle of the concrete slab. The convective heat transfer coefficient between the floor and the air is a constant value based on the European standard (UNI EN 1264-5) (2009).

Figure 12 shows the comparison with the RMSE, significance index and correlation index for the radiant floor agent models and Figure 13 presents the estimation and validation results. The significance and correlation index of model 2 and 3 did not provide clear evidence for the model

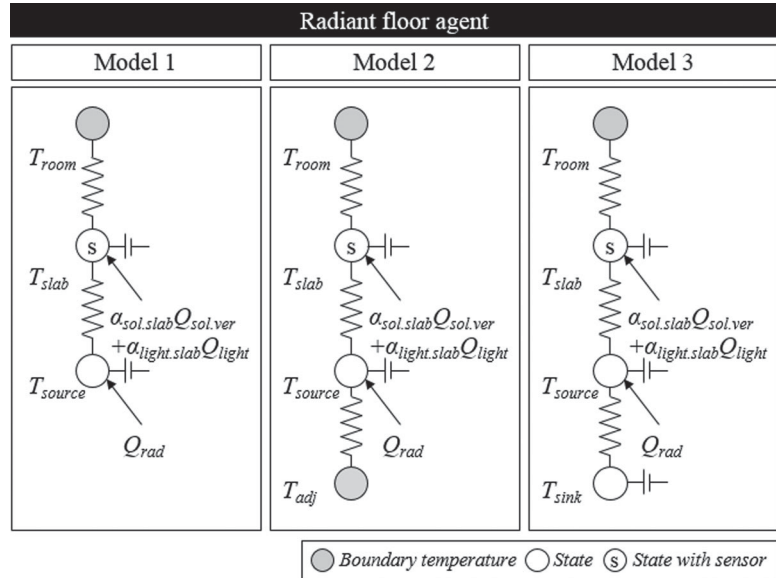


Figure 11. Structure of radiant floor agent models.

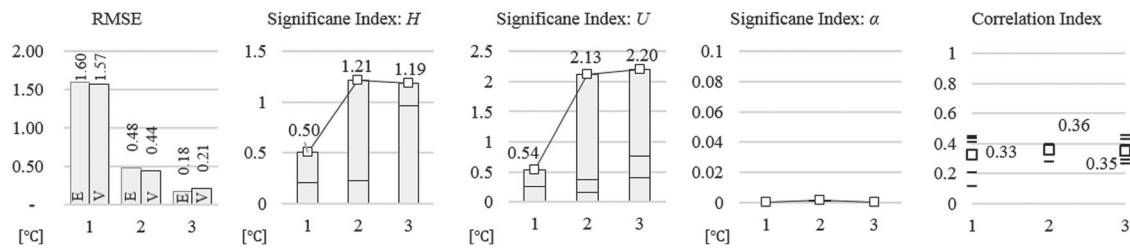


Figure 12. Model comparison of radiant floor agent (E and V represent estimation and validation).

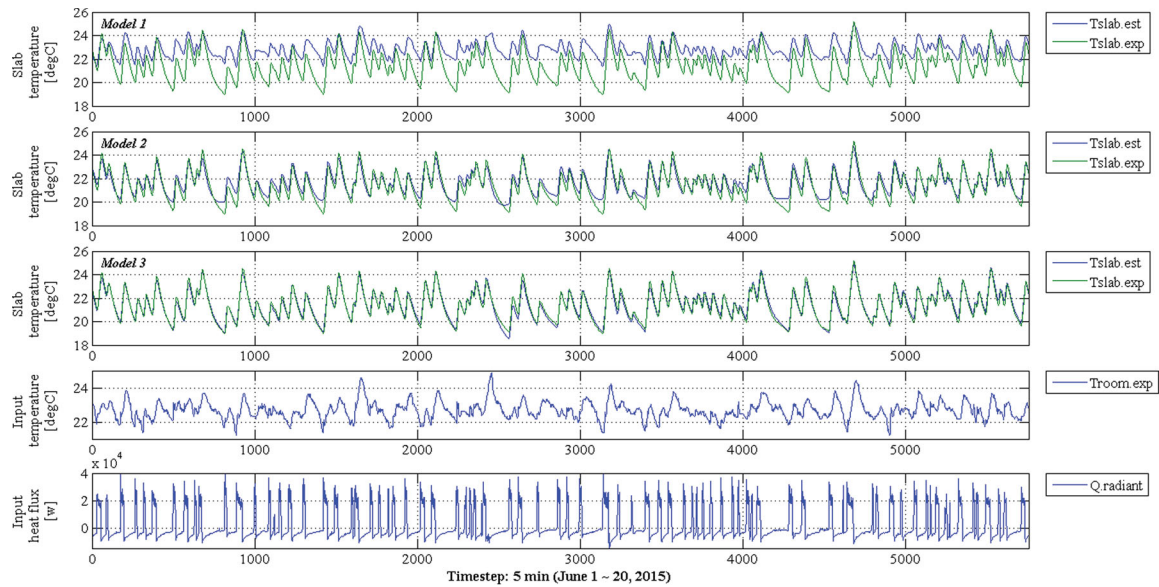


Figure 13. Estimation (1–1440) and validation (1441–5760) results for the radiant floor agent models.

selection. The RMSE was sufficient to discard model 1; its predictions does not follow the experimental data because its structure is too simple to reflect the actual heat transfer phenomena below the slab. On the contrary, models 2 and 3 could capture this dynamics using a constant temperature for the adjacent zone or an additional state. Model 3, shows the best performance, as its prediction follows the experiment trajectory with low error for the entire period so it was selected to be the best model. The significance index for  $\alpha$  is very small that it is neglected in the integrated model.

#### 4.2.3. Room agent

Three sub-system model structures are considered for the room agent including first-, second- and third-order models (Figure 14). The outdoor air temperature ( $T_{out}$ ) is used as a boundary temperature along with the two temperatures from the two adjacent agents of the double façade ( $T_{cav}$ ) and radiant floor ( $T_{slab}$ ).  $T_{env}$ ,  $T_{ext.env}$  and  $T_{int.env}$  are envelope temperatures considered in models 2 and 3 (Figure 14). The transmitted and incident solar radiation ( $Q_{sol.ver}$  and  $Q_{sol.hor}$ , respectively) and lighting ( $Q_{light}$ ) heat gains are used as disturbance inputs multiplied by the corresponding coefficients ( $\alpha_{sol.room}$ ,  $\alpha_{sol.env}$ ,  $\alpha_{sol.ext.env}$  and  $\alpha_{light.room}$ ). The internal heat gain ( $Q_{int,heat}$ ) consists of heat flux values for computers, monitors and people (adopted from Hosni, Jones, and Xu 1999; Wilkins and Hosni 2011).  $Q_{int,heat}$  is multiplied by the heat flux coefficient ( $\alpha_{ppl}$ ), which represents the number of people and it is an estimate parameter. The heat flux from the air handling unit ( $Q_{AHU}$ ) is an input to the room air temperature ( $T_{room}$ ). The

room air temperature varies according to the temperature difference with adjacent mediums through convection and radiation. However, relatively direct changes are made due to AHU since a portion of the room air is displaced with heating and cooling injection. Therefore, the inverse of the air capacity in the input matrix ( $B$ ), which is multiplied to the heat flux input from the air system of the state-space equation, is treated as a separate estimate parameter in addition to that in the state matrix ( $A$ ). The first-order model considers only the room air temperature as state variable, which can be justified by the fact that is a high performance building so the external wall is well insulated (including two insulation layers and the air space). The second- and third-order models are more detailed in terms of including the inputs to the state that represents the envelope temperature. All initial values are from the European standard (UNI EN 1264-5) (2009), literature (Park et al. 2004) and TRNSYS type 56 (TRNSYS 17 2010) for the floor surface, wall surface and double façade side surface, respectively.

Figure 15 shows the comparison with the RMSE, significance index and correlation index for the room agent models and Figure 16 presents the estimation and validation results. All models are good in terms of the RMSE. However, model 1 is less accurate than models 2 and 3, and all significance indices are lower because the resistance between outdoors and the room, and the coefficients multiplied to  $Q_{light}$  and  $Q_{solar}$  are very small and could be neglected. Model 3 has lower significance indices and larger correlation indices compared to model 2. Therefore, model 2 has been selected to be the best model.

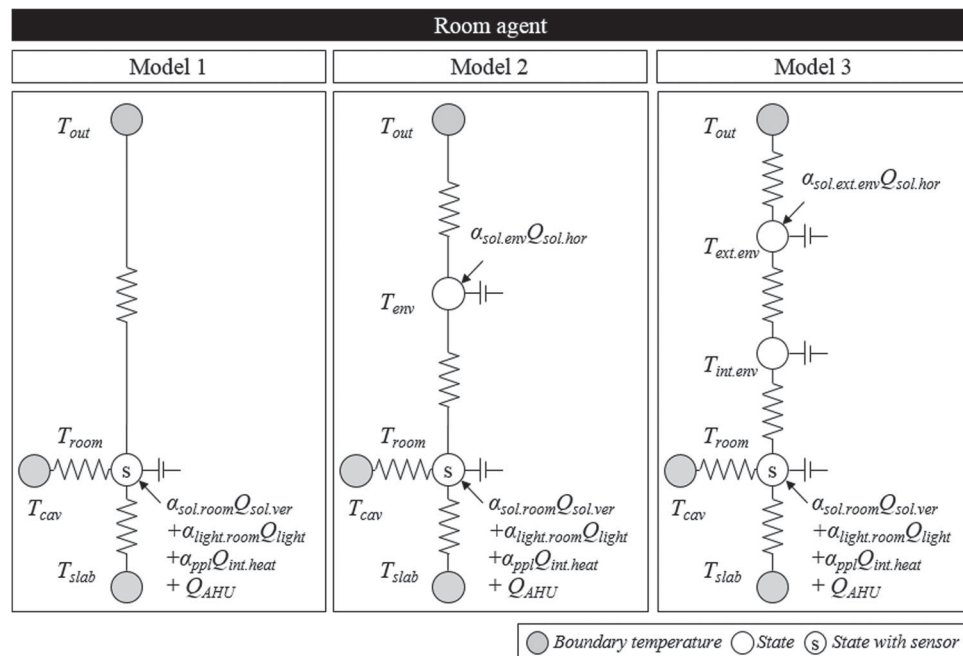


Figure 14. Structure of room agent models.

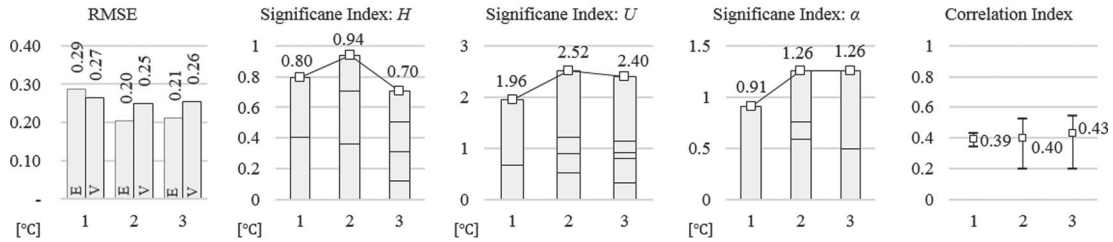


Figure 15. Model comparison of room agent (E and V represent estimation and validation).

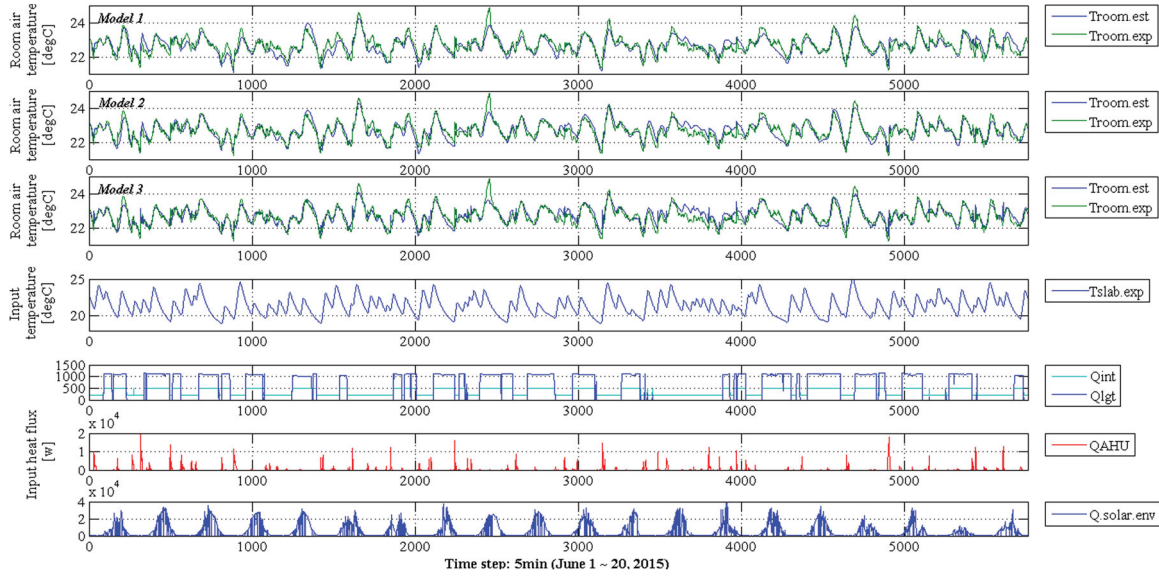


Figure 16. Estimation (1–1440) and validation (1441–5760) results for the room agent models.

#### 4.3. Integrated-system model

Figure 17 shows the thermal network of the integrated-system agent. The first-, third- and second-order models from the double façade, radiant floor and room agent are assembled to the integrated-system agent. It has one boundary temperature corresponding to the outdoor air ( $T_{out}$ ) and six states; three of them, that is, the cavity air ( $T_{cav}$ ), room air ( $T_{room}$ ) and slab temperature ( $T_{slab}$ ) have information from sensor data. Two different models are discussed in the following sections.

##### 4.3.1. Negotiated-shared parameter model

Table 3 shows the dual decomposition algorithm for this case-study.  $i, j$  and  $k$  represent double façade, radiant floor and room agent. All values and procedures were set as explained in the methodology (Section 3.4). The number of the estimated variables are 4, 7 and 12 for the double façade agent, radiant floor agent and room agent, respectively. Two of them are shared parameters (complicating variables) which result in four copies for three sub-system agents; one for the double façade agent, one for the radiant floor agent and two for the room agent. Therefore, it is a sparse problem in terms of the number of complicating

variables (2) compared to that of all variables (23) and reasonable to apply the decomposition theory.

Figure 18 shows the evolution of shared parameters (upper two graphs) and dual variables (lower two graphs). The first shared parameter ( $\theta_{ij(i)}$  and  $\theta_{ij(j)}$ ), which is the inverse of resistance between the double façade agent and room agent, is converged in fourteenth iterations. The second shared parameter ( $\theta_{jk(j)}$  and  $\theta_{jk(k)}$ ), the resistance between the room agent and radiant floor agent, is converged in eighth iterations. In the meantime, the two dual variables ( $\lambda_{ij}$  and  $\lambda_{jk}$ ) are converged to a constant value.

Figure 19 represents the estimation and validation results of negotiated-shared parameter model. The three upper graphs show the comparison between the model prediction (blue line) and the experiment (green line) for the three agents. The two lower graphs present the exogenous and control input, which are the outdoor air temperature and heat flux input from the air system, solar radiation and radiant floor system. The RMSE of the estimation period is  $2.16^{\circ}\text{C}$ ,  $0.29^{\circ}\text{C}$  and  $0.24^{\circ}\text{C}$ , and that of the validation period is  $1.71^{\circ}\text{C}$ ,  $0.46^{\circ}\text{C}$  and  $0.37^{\circ}\text{C}$  for cavity air, room air and slab temperature, respectively. The estimation result is fairly robust and stable as the validation maintains its good prediction even for a period of 20 days which was

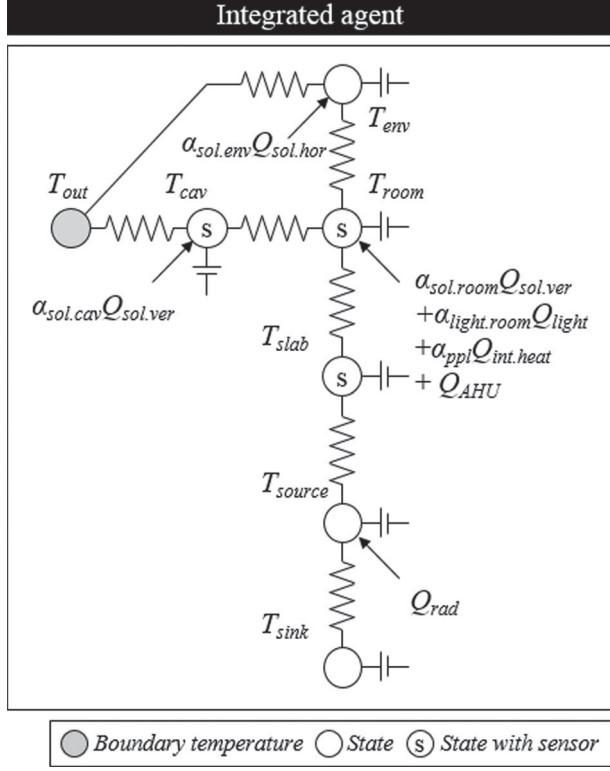


Figure 17. Structure of integrated agent model.

considered to test the model, as information about the internal heat gain due to equipment and occupancy schedule was not available, and also the final integrated model is not estimated but built based on the information from the sub-system (agent) models. Estimated values for all parameters are presented in Table 4.

Table 3. Dual decomposition algorithm for the case-study.

$$\begin{aligned}
 & \text{while } \theta_{ij(i)}^{k+1} = \theta_{ij(j)}^{k+1} \text{ and } \theta_{jk(j)}^{k+1} = \theta_{jk(k)}^{k+1} \\
 & \theta_i^{k+1} = \underset{\theta_i^k}{\operatorname{argmin}} \left( g_i(\theta_i^k) + \lambda_{ij}^k \theta_{ij(i)}^k \right) \\
 & \theta_j^{k+1} = \underset{\theta_j^k}{\operatorname{argmin}} \left( g_j(\theta_j^k) - \lambda_{ij}^k \theta_{ij(j)}^k + \lambda_{jk}^k \theta_{jk(j)}^k \right) \\
 & \theta_k^{k+1} = \underset{\theta_k^k}{\operatorname{argmin}} \left( g_k(\theta_k^k) - \lambda_{jk}^k \theta_{jk(k)}^k \right) \\
 & \begin{bmatrix} \lambda_{ij}^{k+1} \\ \lambda_{jk}^{k+1} \end{bmatrix} = \begin{bmatrix} \lambda_{ij}^k \\ \lambda_{jk}^k \end{bmatrix} + \begin{bmatrix} \mu_{ij} & 0 \\ 0 & \mu_{jk} \end{bmatrix} \begin{bmatrix} \theta_{ij(i)}^{k+1} - \theta_{ij(j)}^{k+1} \\ \theta_{jk(j)}^{k+1} - \theta_{jk(k)}^{k+1} \end{bmatrix} \\
 & \text{end}
 \end{aligned}$$

An integrated model (Figure 17) developed based on standard centralized estimation, failed to provide accurate predictions for the room and slab temperatures. Also, integrated models assembled with the agent negotiation approach, did not provide accurate predictions, when sub-system models with inferior performance (e.g. model 2 for the double façade agent, model 1 for the room agent, model 1 for the radiant floor agent), based on the criteria presented in Section 4.2, were used. These two comparisons (results not shown) confirm the merits of the sub-system model evaluation and distributed system identification presented in this work.

Residual analysis including auto-correlation and cross-correlation has been used as post processing for the estimation period. The confidence range is set at  $\pm 0.0517$  based on the 95% confidence standard deviation. Figure 20 shows a sample auto-correlation function of the residual from

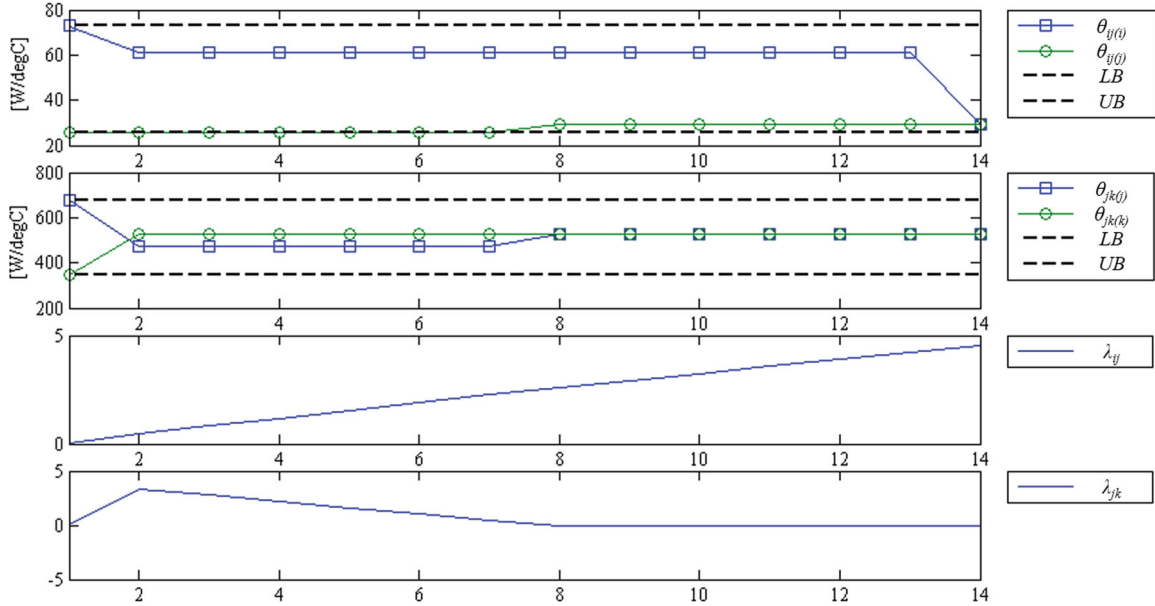


Figure 18. Evolution of shared parameters and dual variables.

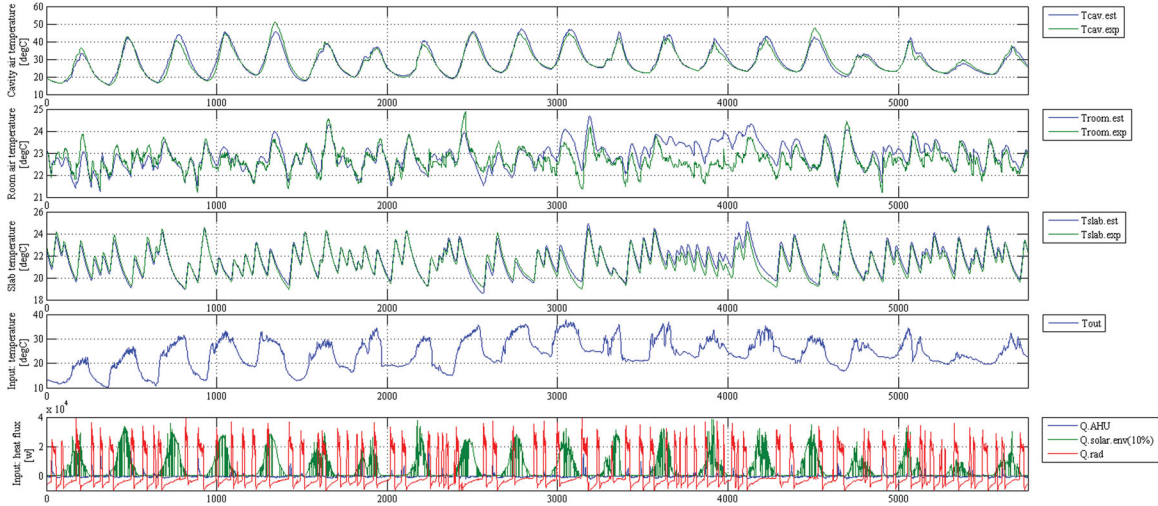


Figure 19. Estimation (1–1440) and validation (1441–5760) results of negotiated-shared parameter model.

Table 4. Estimated values of negotiated-shared parameter model.

$H_{\text{cav}}$	1.13E-6	$U_{\text{out-cav}}$	51.92	$\alpha_{\text{sol.cav}}$	0.08
$H_{\text{slab}}$	3.53E-8	$U_{\text{cav-room}}$	29.07	$\alpha_{\text{sol.room}}$	3.77E-19
$H_{\text{source}}$	3.61E-7	$U_{\text{room-slab}}$	527.58	$\alpha_{\text{sol.env}}$	0.17
$H_{\text{sink}}$	4.14E-17	$U_{\text{slab-source}}$	1402.44	$\alpha_{\text{light.room}}$	0.14
$H_{\text{room}}$	2.43E-7 (rad + conv) 8.00E-8 (conv)	$U_{\text{source-sink}}$	249.39	$\alpha_{\text{ppl}}$	1.91
$H_{\text{env}}$	6.31E-8	$U_{\text{room-env}}$	21.75		
		$U_{\text{out-env}}$	269.36		

Note:  $H$  ( $^{\circ}\text{C}/\text{J}$ ) represents the inverse of capacity corresponding to the temperature node (indicated by the subscript) and  $U$  ( $\text{W}/^{\circ}\text{C}$ ) the inverse of resistance between the temperature nodes in Figure 17.

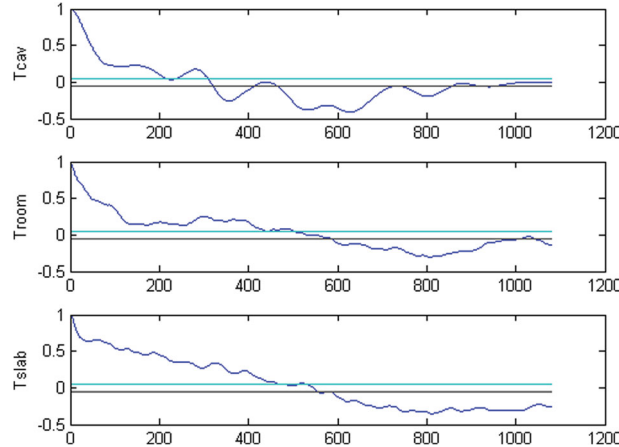


Figure 20. Sample auto-correlation function of the residual (negotiated-shared parameter model).

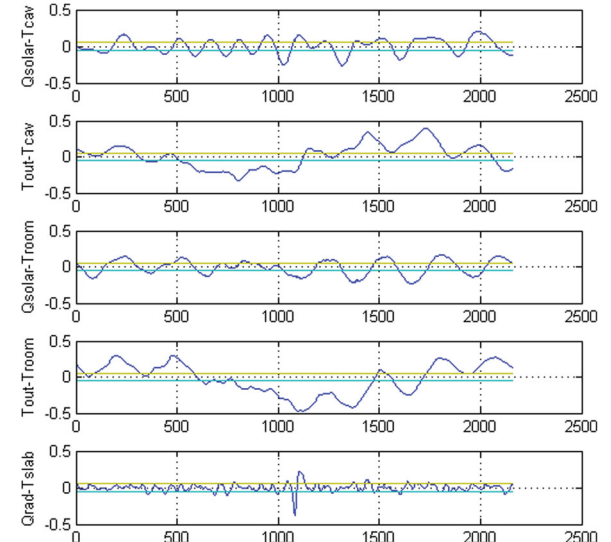


Figure 21. Sample cross-correlation function between input and residual (negotiated-shared parameter model).

each agent and Figure 21 shows a sample cross-correlation function between the input and residual. All of them are outside of the confidence range, which are illustrated as two parallel lines, even though 75% of data length was examined.

#### 4.3.2. Free-shared parameter model

Figure 22 represents the estimation and validation results for the free-shared parameter model. The structure is the same with that explained for Figure 19. The RMSE

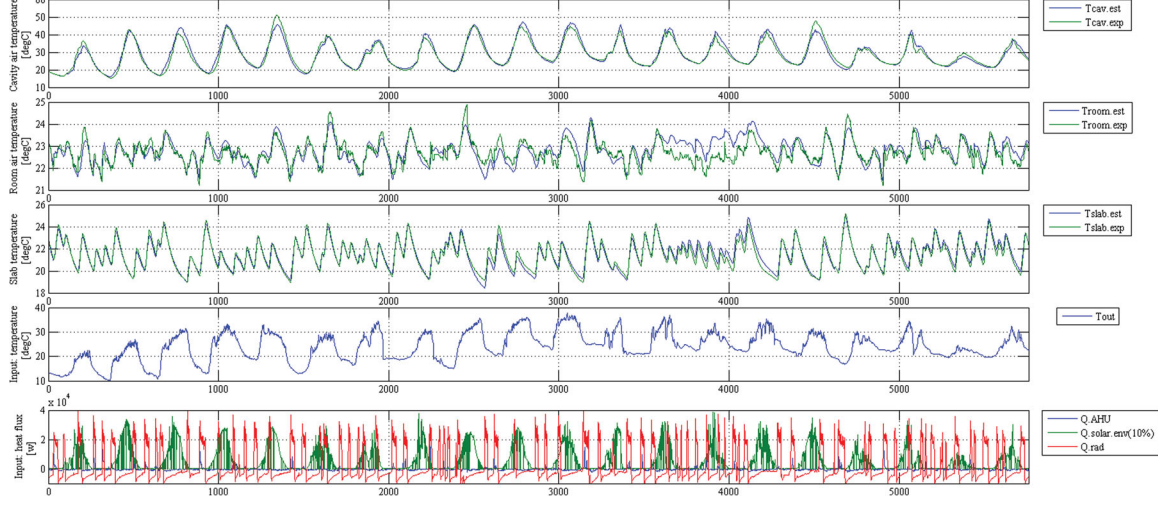


Figure 22. Estimation (1–1440) and validation (1441–5760) results of free-shared parameter model.

Table 5. Estimated values of free-shared parameter model.

$H_{\text{cav}}$	4.68E-07	$U_{\text{out-cav}}$	123.93	$\alpha_{\text{sol.cav}}$	0.19
$H_{\text{slab}}$	3.47E-08	$U_{\text{cav-room}}$	72.87 (double façade agent)	$\alpha_{\text{sol.room}}$	1.89E-17
$H_{\text{source}}$	3.48E-07		25.48 (room agent)	$\alpha_{\text{sol.env}}$	0.17
$H_{\text{sink}}$	4.63E-12	$U_{\text{room-slab}}$	679.76 (room agent)	$\alpha_{\text{light.room}}$	0.18
$H_{\text{room}}$	1.97E-7 (rad + conv) 7.91E-8 (conv)	$U_{\text{slab-source}}$	345.24 (radiant floor agent)	$\alpha_{\text{ppl}}$	2.74
$H_{\text{env}}$	8.37E-08	$U_{\text{source-sink}}$	1371.31		
		$U_{\text{room-env}}$	280.28		
		$U_{\text{out-env}}$	34.4		
			300.43		

Note:  $H$  ( $^{\circ}\text{C}/\text{J}$ ) represents the inverse of capacity corresponding to the temperature node (indicated by the subscript) and  $U$  ( $\text{W}/^{\circ}\text{C}$ ) the inverse of resistance between the temperature nodes in Figure 17.

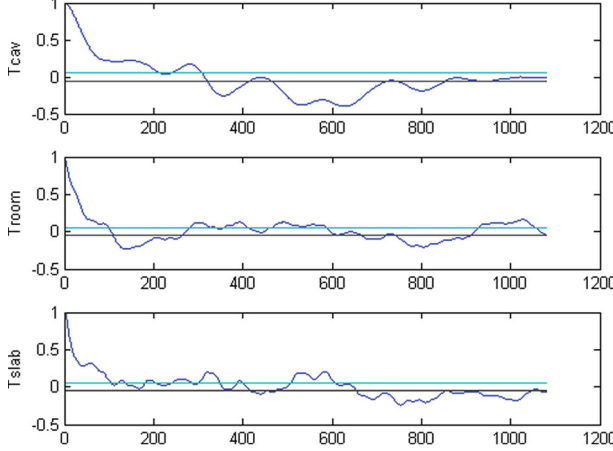


Figure 23. Sample auto-correlation function of residual (free-shared parameter model).

of the estimation period is  $2.16^{\circ}\text{C}$ ,  $0.23^{\circ}\text{C}$  and  $0.15^{\circ}\text{C}$ , and that of the validation period is  $1.68^{\circ}\text{C}$ ,  $0.36^{\circ}\text{C}$  and  $0.30^{\circ}\text{C}$  for the cavity air, room air and slab temperature, respectively. The prediction of the free-shared parameter model is slightly better than that of the negotiated-shared parameter model in both the estimation and validation

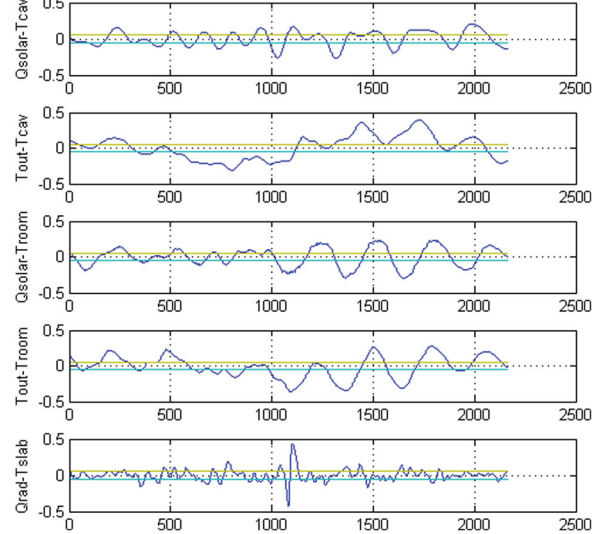


Figure 24. Sample cross-correlation function between input and residual (free-shared parameter model).

period. Therefore, it has been shown that the physical meaning of the shared parameter model is compensated with a small loss in accuracy of the prediction, which however, is not significant considering the complexity of the

integrated-system model. Estimated values for all parameters are presented in Table 5. Figures 23 and 24 show the sample auto-correlation and cross-correlation function for the free-shared parameter model, based on the same setting and structure used in the negotiated-shared parameter model. All results are generally similar with those obtained with the negotiated-shared parameter model but the auto-correlation of the room agent and the radiant floor agent are slightly better than the negotiated-shared parameter model.

## 5. Conclusions

In this paper, an agent-based estimation framework for data-driven building models has been introduced. An experimental case-study of a single-zone occupied office space with multiple sub-systems (radiant floor, double façade, AHU) has been used to demonstrate the new approach. The results indicate that the agent-based estimation is a potential solution for control-oriented models of building systems that can be easier to develop and integrate whereas the conventional centralized approach could not provide accurate predictions for all states. The main conclusions are summarized as follows:

- Sensitivity-based parameter range selection and shift was implemented and the optimization results for the sub-systems grey-box model estimation show that the chance for a global minimum is increased. Different structures of sub-system models were compared and the selection criteria based on model prediction error as well as the parameter sensitivity to output trajectory and parameter correlation proved to guarantee the accuracy of the integrated-system model.
- Integrated -system models were assembled based on distributed and decentralized method. The distributed model requires the negotiation for the shared parameter but the decentralized model uses a different parameter value from sub-system agents. Both models show fairly good prediction accuracy in the validation set. However, in the free- shared parameter model the physical meaning may be compromised.
- The residual analysis of auto-correlation and cross-correlation for both integrated agent models show that even though the residuals are small, the 95% confidence range for experiment-based estimation with unmeasured uncertainty due to occupancy and internal heat gains cannot be met.

The experimental datasets used in this study are confined to the summer season although cooling and heating were used alternately. To overcome this limitation, adaptive estimation could be implemented in the future. The agent-based estimation is a suitable approach for this

implementation. For example, each agent could incorporate adaptive parameters that need to be updated according to environmental conditions, such as outdoor air temperature and control scheme. All sub-agents would be self-tuned by validating their prediction with measured data.

In this paper, the proposed framework was demonstrated for a case-study with terminal comfort delivery. In the future, the methodology could be extended to other building systems and could be packaged into a toolbox integrated in BMS. With regards to the specific case-study of terminal comfort delivery with radiant floor heating and cooling, on-going work performed by the authors is focused on the deployment of the agent-based models in predictive controllers.

## Acknowledgements

The authors would like to thank Prof. Jianghai Hu, Xiaodong Hou and Yingying Xiao (School of Electrical and Computer Engineering, Purdue) as well as Prof. Jim Braun and Dr Jie Cai (School of Mechanical Engineering, Purdue) for the fruitful discussions on this topic.

## Funding

This work was funded by the National Science Foundation [grant number 1329875]. Any opinions, findings and conclusions or recommendations expressed in this material are those of the authors and do not necessarily reflect the views of the National Science Foundation.

## Nomenclature

$A$	state matrix
$B$	input matrix
$C$	output matrix
$CI$	correlation index
$Cp$	capacitance [J/kg °C]
$f$	objective function
$g$	normalized objective function
$h$	lag for auto- and cross-correlation
$k$	time-step
$K$	covariance
$M$	Markov parameter sequence
$m$	number of parameters in agent
$n$	number of iterations
$R$	thermal resistance [°C/W]
$r$	residual
$S$	sensitivity matrix
$\tilde{S}$	reduced sensitivity matrix
$\bar{S}$	Averaged value of reduced sensitivity matrix
$SI$	sensitivity index
$T$	temperature
$u$	input vector
$X$	state temperature [°C]
$y$	measured output temperature value [°C]
$Y$	measured output temperature vector [°C]
$\hat{y}$	predicted output temperature value [°C]
$\hat{Y}$	predicted output temperature vector [°C]
$\alpha$	heat flux coefficient
$\gamma$	bound range

$\varepsilon$	stop range
$\theta$	estimate parameter
$\lambda$	dual variable for decomposition
$\mu$	time-step for decomposition
$\rho$	correlation coefficient

### Subscripts/superscripts

$*$	optimal
$d$	discrete version of the state-space matrices
$i$	agent $i$
$ij(i)$	local copy of shared parameter between agent $i$ and $j$ in agent $i$
$ij(j)$	local copy of shared parameter between agent $i$ and $j$ in agent $j$
$j$	agent $j$
$jk(j)$	local copy of shared parameter between agent $j$ and $k$ in agent $j$
$jk(k)$	local copy of shared parameter between agent $j$ and $k$ in agent $k$
$k$	agent $k$ /time-step
$LB$	lower bound
$n_{Cp}$	number of parameter $Cp$
$n_H$	number of parameter $H$
$n_R$	number of parameter $R$
$n_U$	number of parameter $U$
$n_\alpha$	number of parameter $\alpha$
$p,q$	parameter in agent
std	standard deviation
$UB$	upper bound

### References

- Agbi, Clarence, Zhen Song, and Bruce Krogh. 2012. “Parameter Identifiability for Multi-zone Building Models.” *Proceedings of the IEEE Conference on Decision and Control*: 6951–6956. doi:10.1109/CDC.2012.6425995.
- Bacher, Peder, and Henrik Madsen. 2011. “Identifying Suitable Models for the Heat Dynamics of Buildings.” *Energy and Buildings* 43 (7): 1511–1522. doi:10.1016/j.enbuild.2011.02.005.
- Bengea, Sorin C., Anthony D. Kelman, Francesco Borrelli, Russell Taylor, and Satish Narayanan. 2014. “Implementation of Model Predictive Control for an HVAC System in a Mid-size Commercial Building.” *HVAC&R Research* 20 (1): 121–135. doi:10.1080/10789669.2013.834781.
- Berthou, Thomas, Pascal Stabat, Raphael Salvazet, and Dominique Marchio. 2014. “Development and Validation of a Grey-box Model to Predict Thermal Behavior of Occupied Office Buildings.” *Energy and Buildings* 74 (5): 91–100. doi:10.1016/j.enbuild.2014.01.038.
- Braun, James, and Nitin Chaturvedi. 2002. “An Inverse Grey-box Model for Transient Building Load Prediction.” *HVAC&R Research* 8 (1): 73–99. doi:10.1080/10789669.2002.10391290.
- Braun, J. E., K. W. Montgomery, and N. Chaturvedi. 2001. “Evaluating the Performance of Building Thermal Mass Control Strategies.” *HVAC&R Research* 7 (4): 403–428. doi:10.1080/10789669.2001.10391283.
- Cai, Jie, and James Braun. 2015. “An Inverse Hygrothermal Model for Multi-zone Buildings.” *Journal of Building Performance Simulation* 1493 (11): 1–19. doi:10.1080/19401493.2015.1108999.
- Cai, Jie, Donghun Kim, James E. Braun, and Jianghai Hu. 2016. “Optimizing Zone Temperature Setpoint Excitation to Minimize Training Data for Data-driven Dynamic Building Models.” *Proceedings of the American Control Conference*.
- Cai, Jie, Donghun Kim, Vamsi K. Putta, James E. Braun, and Jianghai Hu. 2015. “Multi-agent Control for Centralized Air Conditioning Systems Serving Multi-zone Buildings.” *Proceedings of the American Control Conference*: 986–993. doi:10.1109/ACC.2015.7170862.
- Cigler, Jiří, Samuel Prívara, Zdeněk Váňa, Eva Žáčeková, and Lukáš Ferkl. 2012. “Optimization of Predicted Mean Vote Index within Model Predictive Control Framework: Computationally Tractable Solution.” *Energy and Buildings* 52: 39–49. doi:10.1016/j.enbuild.2012.05.022.
- Corbin, Charles D., Gregor P. Henze, and Peter May-Ostendorp. 2012. “A Model Predictive Control Optimization Environment for Real-time Commercial Building Application.” *Journal of Building Performance Simulation* 1493: 1–16. doi:10.1080/19401493.2011.648343.
- Davidsson, Paul, and Magnus Boman. 2005. “Distributed Monitoring and Control of Office Buildings by Embedded Agents.” *Information Sciences* 171 (4): 293–307. doi:10.1016/j.ins.2004.09.007.
- De Coninck, Roel, and Lieve Helsen. 2016. “Practical Implementation and Evaluation of Model Predictive Control for an Office Building in Brussels.” *Energy and Buildings* 111 (1): 290–298. doi:10.1016/j.enbuild.2015.11.014.
- De Coninck, Roel, Fredrik Magnusson, Johan Åkesson, and Lieve Helsen. 2015. “Toolbox for Development and Validation of Grey-box Building Models for Forecasting and Control.” *Journal of Building Performance Simulation* 1493 (July): 1–16. doi:10.1080/19401493.2015.1046933.
- Del Barrio, Elena Palomo, and Gilles Guyon. 2003. “Theoretical Basis for Empirical Model Validation using Parameters Space Analysis Tools.” *Energy and Buildings* 35 (10): 985–996. doi:10.1016/S0378-7788(03)00038-0.
- Del Barrio, Elena Palomo, and Gilles Guyon. 2004. “Application of Parameters Space Analysis Tools for Empirical Model Validation.” *Energy and Buildings* 36 (1): 23–33. doi:10.1016/S0378-7788(03)00039-2.
- Doren, Jorn F. M. Van, Sippe G. Douma, Paul M. J. Van den Hof, Jan Dirk Jansen, and Okko H. Bosgra. 2009. “Identifiability: From Qualitative Analysis to Model Structure Approximation.” *Proceedings of the 15th International Federation on Automatic Control (IFAC) Symposium on System Identification*: 664–669. doi:10.3182/20090706-3-FR-2004.00110.
- Duan, Jianmin, and Gilles Fan Lin. 2008. “Research of Intelligent Building Control Using an Agent-based Approach.” *6th IEEE International Conference on Industrial Informatics*: 991–994. doi:10.1109/INDIN.2008.4618246.
- European Standard (UNI EN 1264-5). 2009. “Water Based Surface Embedded Heating And Cooling Systems – Part 5: Heating and Cooling Surfaces Embedded In Floors, Ceilings and Walls – Determination of the Thermal Output.” [http://www.eurotherm.info/ww/normativa/uni\\_en\\_1264\\_5](http://www.eurotherm.info/ww/normativa/uni_en_1264_5).
- Feng, Jingjuan, Frank Chuang, Francesco Borrelli, and Fred Bau man. 2015. “Model Predictive Control of Radiant Slab Systems with Evaporative Cooling Sources.” *Energy and Buildings* 87 (1): 199–210. doi:10.1016/j.enbuild.2014.11.037.
- Gwerder, Markus, and Dimitrios Gyalistras. 2013. *Final Report: Use of Weather and Occupancy Forecasts for Optimal Building Climate Control – Part II: Demonstration (OptiControl-II)*. Zürich: ETH Zürich.
- Hazyuk, Ion, Christian Ghiaus, and David Penhouet. 2012. “Optimal Temperature Control of Intermittently Heated Buildings using Model Predictive Control: Part I – Building Modeling.” *Building and Environment* 51 (5): 379–387. doi:10.1016/j.buildenv.2011.11.009.

- Henze, Gregor P. 2013. "Model Predictive Control for Buildings: A Quantum Leap?" *Journal of Building Performance Simulation* 6 (3): 157–158. doi:10.1080/19401493.2013.778519.
- Hosni, Mohammad H., Byron W. Jones, and Hanming Xu. 1999. "Experimental Results for Heat Gain and Radiant/convective Split from Equipment in Buildings." *ASHRAE Transactions* 105: 1–13.
- Hu, Jianjun, and Panagiota Karava. 2014. "A State-space Modeling Approach and Multi-level Optimization Algorithm for Predictive Control of Multi-zone Buildings with Mixed-mode Cooling." *Building and Environment* 80 (October): 259–273. doi:10.1016/j.buildenv.2014.05.003.
- Jennings, N. R., and S. Bussmann. 2003. "Agent-based Control System: Why are They Suited to Engineering Complex Systems?" *IEEE Control Systems* 23 (3): 61–73. doi:10.1109/MCS.2003.1200249.
- Jiménez, M. J., H. Madsen, and K. K. Andersen. 2008. "Identification of the Main Thermal Characteristics of Building Components using MATLAB." *Building and Environment* 43 (2): 170–180. doi:10.1016/j.buildenv.2006.10.030.
- Kelly, George E., and Steven T. Bushby. 2012. "Are Intelligent Agents the Key to Optimizing Building HVAC System Performance?" *HVAC&R Research* 18 (4): 750–759. doi:10.1080/10789669.2012.682693.
- Kramer, Rick, Jos van Schijndel, and Henk Schellen. 2013. "Inverse Modeling of Simplified Hygrothermal Building Models to Predict and Characterize Indoor Climates." *Building and Environment* 68 (10): 87–99. doi:10.1016/j.buildenv.2013.06.001.
- Lacroix, Benoit, Liten Ines, and David Mercier. 2012. "Multi-agent Control of Thermal Systems in Buildings." Proceedings of Agent Technologies in Energy Systems (ATES@AAMAS'12), Valencia, Spain.
- Lehmann, B., D. Gyalistras, M. Gwerder, K. Wirth, and S. Carl. 2013. "Intermediate Complexity Model for Model Predictive Control of Integrated Room Automation." *Energy and Buildings* 58 (3): 250–262. doi:10.1016/j.enbuild.2012.12.007.
- Li, Siwei, Jaewan Joe, Jianjun Hu, and Panagiota Karava. 2015. "System Identification and Model-predictive Control of Office Buildings with Integrated Photovoltaic-thermal Collectors, Radiant Floor Heating and Active Thermal Storage." *Solar Energy* 113 (March): 139–157. doi:10.1016/j.solener.2014.11.024.
- Li, Xiwang, and Jin Wen. 2014. "Building Energy Consumption On-line Forecasting using Physics Based System Identification." *Energy and Buildings* 82 (10): 1–12. doi:10.1016/j.enbuild.2014.07.021.
- Ljung, L. 1999. *System Identification: Theory for the User*. Upper Saddle River, NJ: Prentice Hall.
- Ma, Yudong, Garrett Anderson, and Francesco Borrelli. 2011. "A Distributed Predictive Control Approach to Building Temperature Regulation." *American Control Conference*: 2089–2094. doi:10.1109/ACC.2011.5991549.
- Ma, Y., Francesco Borrelli, and Brandon Hency. 2012. "Model Predictive Control for the Operation of Building Cooling Systems." *IEEE Transactions on Control Systems Technology* 20 (3): 796–803. doi:10.1109/TCST.2011.2124461.
- Ma, Yudong, Anthony Kelman, Allan Daly, and Francesco Borelli. 2012. "Predictive Control for Energy Efficient Buildings with Thermal Storage." *IEEE Control Systems*. February: 44–64. doi:10.1109/MCS.2011.2172532.
- Ma, Yudong, Jadranko Matuško, and Francesco Borrelli. 2014. "Stochastic Model Predictive Control for Building HVAC Systems: Complexity and Conservatism." *IEEE Transactions on Control Systems Technology* 23 (1): 1–16. doi:10.1109/TCST.2014.2313736.
- Mathworks. 2015. *Optimization Toolbox: User's Guide (r2015b)*. Natick: MathWorks <http://www.mathworks.com/wp-content/uploads/2011/09/Sept-05-Heat-Gain-Split.pdf>.
- Mo, ZhengChun. 2003. "An Agent-based Simulation-assisted Approach to Bi-lateral Building Systems Control." ProQuest Dissertations and Theses 3111479: 84 p.
- Mokhtar, Maizura, Matthew Stables, Xiongwei Liu, and Joe Howe. 2013. "Intelligent Multi-agent System for Building Heat Distribution Control with Combined Gas Boilers and Ground Source Heat Pump." *Energy and Buildings* 62 (7): 615–626. doi:10.1016/j.enbuild.2013.03.045.
- Moroşan, Petru-Daniel, Romain Bourdais, Didier Dumur, and Jean Buisson. 2010a. "Building Temperature Regulation using a Distributed Model Predictive Control." *Energy and Buildings* 42 (9): 1445–1452. doi:10.1016/j.enbuild.2010.03.014.
- Moroşan, Petru Daniel, Romain Bourdais, Didier Dumur, and Jean Buisson. 2010b. "Distributed Model Predictive Control Based on Benders' Decomposition Applied to Multisource Multizone Building Temperature Regulation." *Proceedings of the IEEE Conference on Decision and Control*: 3914–3919. doi:10.1109/CDC.2010.5717092.
- Necoara, Ion, Valentin Nedelcu, and Ioan Dumitache. 2011. "Parallel and Distributed Optimization Methods for Estimation and Control in Networks." *Journal of Process Control* 21 (5): 756–766. doi:10.1016/j.jprocont.2010.12.010.
- Nedíc, Angelia, and Asuman Ozdaglar. 2009. "Cooperative Distributed Multi-agent Optimization." In *Convex Optimization in Signal Processing and Communications*, edited by Palomar, D. P. and Y. C. Eldar, 340–386. New York: Cambridge University Press.
- Negenborn, R. R., and J. M. Maestre. 2014. "Distributed Model Predictive Control: An Overview and Roadmap of Future Research Opportunities." *IEEE Control Systems* 34 (August): 87–97. doi:10.1109/MCS.2014.2320397.
- Nghiêm, Truong X., Madhur Behl, George J. Pappas, and Rahul Mangharam. 2012. "Green Scheduling for Radiant Systems in Buildings." *Proceedings of the IEEE Conference on Decision and Control*: 7577–7582. doi:10.1109/CDC.2012.6426318.
- Nghiêm, Truong X., George J. Pappas, and Rahul Mangharam. 2013. "Event-based Green scheduling of radiant systems in buildings." *Proceedings of the American Control Conference*: 455–460, June 17–19. doi:10.1109/ACC.2013.6579879.
- Oldewurtel, Frauke, Alessandra Parisio, Colin N. Jones, Dimitrios Gyalistras, Markus Gwerder, Vanessa Stauch, Beat Lehmann, and Manfred Morari. 2012. "Use of Model Predictive Control and Weather Forecasts for Energy Efficient Building Climate Control." *Energy and Buildings* 45 (2): 15–27. doi:10.1016/j.enbuild.2011.09.022.
- Park, Cheol-Soo, Godfried Augenbroe, Tahar Messadi, Mate Thitisawat, and Nader Sadegh. 2004. "Calibration of a Lumped Simulation Model for Double-skin Façade Systems." *Energy and Buildings* 36 (11): 1117–1130. doi:10.1016/j.enbuild.2004.04.003.
- Prívara, Samuel, Jiří Cigler, Zdeněk Váňa, Frauke Oldewurtel, Carina Saggerschnig, and Eva Žáčeková. 2013. "Building Modeling as a Crucial Part for Building Predictive Control." *Energy and Buildings* 56 (1): 8–22. doi:10.1016/j.enbuild.2012.10.024.
- Prívara, Samuel, Zdeněk Váňa, Eva Žáčeková, and Jiří Cigler. 2012. "Building Modeling: Selection of the Most Appropriate Model for Predictive Control." *Energy and*

- Buildings* 55 (12): 341–350. doi:10.1016/j.enbuild.2012.08.040.
- Putta, Vamsi, Donghun Kim, Jie Cai, Jianghai Hu, James Braun. 2014. “Distributed Model Predictive Control for Building HVAC Systems – A Case Study.” International High Performance Buildings Conference, Purdue University, West Lafayette, July 14–17.
- Reynders, G., J. Diriken, and D. Saelens. 2014. “Quality of Grey-box Models and Identified Parameters as Function of the Accuracy of Input and Observation Signals.” *Energy and Buildings* 82 (10): 263–274. doi:10.1016/j.enbuild.2014.07.025.
- Royer, Sullivan, Stéphane Thil, Thierry Talbert, and Monique Polit. 2014. “A Procedure for Modeling Buildings and Their Thermal Zones using Co-simulation and System Identification.” *Energy and Buildings* 78 (8): 231–237. doi:10.1016/j.enbuild.2014.04.013.
- Samar, S., Stephen Boyd, and Dimitry Gorinevsky. 2007. “Distributed Estimation via Dual Decomposition.” *Proceedings of European Control Conference*: 1511–1516. <https://www.stanford.edu/~boyd/papers/pdf/distrestimecc.pdf>.
- Sharples, Sue, Vic Callaghan, and Graham Clarke. 1999. “A Multi-agent Architecture for Intelligent Building Sensing and Control a Multi-agent Architecture for Intelligent Building Sensing and Control.” *International Sensor Review Journal* May: 1–8. doi:10.1108/02602289910266278.
- Simoes, M. Godoy, and Saurav Bhattacharai. 2011. “Multi Agent-based Energy Management Control for Commercial Buildings.” *2011 IEEE Industry Applications Society Annual Meeting*: 1–6. doi:10.1109/IAS.2011.6074360.
- Sourbron, Maarten, Clara Verhelst, and Lieve Helsen. 2013. “Building Models for Model Predictive Control of Office Buildings with Concrete Core Activation.” *Journal of Building Performance Simulation* 6 (3): 175–198. doi:10.1080/19401493.2012.680497.
- Sun, Biao, Peter B. Luh, Qing Shan Jia, Ziyan Jiang, Fulin Wang, and Chen Song. 2010. “An Integrated Control of Shading Blinds, Natural Ventilation, and HVAC Systems for Energy Saving and Human Comfort.” *2010 IEEE International Conference on Automation Science and Engineering, CASE 2010*: 7–14. doi:10.1109/COASE.2010.5584637.
- Široký, Jan, Frauke Oldewurtel, Jiří Cigler, and Samuel Prívara. 2011. “Experimental Analysis of Model Predictive Control for an Energy Efficient Building Heating System.” *Applied Energy* 88 (9): 3079–3087. doi:10.1016/j.apenergy.2011.03.009.
- Treado, S. J. 2010. “An Agent-based Methodology for Optimizing Building HVAC System Performance.” *ASHRAE 2010 Annual Conference*: 124–134.
- Treado, Stephen, and Payam Delgoshaei. 2010. “Agent-based Approaches for Adaptive Building HVAC System Control.” International High Performance Buildings Conference, Purdue University, West Lafayette, July 12–15.
- Tridium Inc. *Niagara AX Software*. <http://www.tridium.com/>.
- TRNSYS 17. 2010. *Solar Energy Laboratory*. Madison: University of Wisconsin-Madison.
- West, Samuel R., John K. Ward, and Josh Wall. 2014. “Trial Results from a Model Predictive Control and Optimisation System for Commercial Building HVAC.” *Energy and Buildings* 72 (4): 271–279. doi:10.1016/j.enbuild.2013.12.037.
- Wilkins, Christopher K., and Mohammad H. Hosni. 2011. “Plug Load Design Factors.” *ASHRAE Journal* 53 (5): 30–34.
- Yang, Rui, and Lingfeng Wang. 2013. “Multi-zone Building Energy Management using Intelligent Control and Optimization.” *Sustainable Cities and Society* 6 (1): 16–21. doi:10.1016/j.scs.2012.07.001.
- Zhao, Peng, Siddharth Suryanarayanan, and Marcelo Godoy Simões. 2013. “An Energy Management System for Building Structures using a Multi-agent Decision-making Control Methodology.” *IEEE Transactions on Industry Applications* 49 (1): 1–9. doi:10.1109/TIA.2010.5615412.
- Žáčeková, Eva, Zdeněk Váňa, and Jiří Cigler. 2014. “Towards the Real-life Implementation of MPC for an Office Building: Identification Issues.” *Applied Energy* 135 (12): 53–62. doi:10.1016/j.apenergy.2014.08.004.